Journal of Science and Transport Technology
Journal homepage: https://jstt.vn/index.php/en

# A semi-analytical approach for nonlinear vibration of FG-CNTRC doubly curved shallow shells stiffened by FG-CNTRC stiffeners in thermal environment

Cao Cong Anh[1,2], Le Van Kien[3], Nguyen Thi Phuong[4,5*]
[1]University of Transport Ho Chi Minh City, Ho Chi Minh City, Vietnam
[2]Graduate University of Science and Technology, Vietnam Academy of Science and Technology, Hanoi, Vietnam
[3]Mechanics of Advanced Materials and Structures, University of Transport Technology, Hanoi, Vietnam
[4]Mechanics of Advanced Materials and Structures, Institute for Advanced Study in Technology, Ton Duc Thang University, Ho Chi Minh City, Vietnam
[5]Faculty of Civil Engineering, Ton Duc Thang University, Ho Chi Minh City, Vietnam

**Article info**
**Type of article:**
Original research paper

**DOI:**
https://doi.org/10.58845/jstt.utt.2026.en.6.1.347-367

***Corresponding author:**
Email address:
nguyenthiphuong@tdtu.edu.vn

**Received:** 11/10/2025
**Received in Revised Form:** 26/11/2025
**Accepted:** 15/12/2025

**Abstract:** This paper investigates the geometrically nonlinear free and forced vibration behavior of functionally graded carbon nanotube-reinforced composite (FG-CNTRC) doubly curved shallow shells stiffened by FG-CNTRC stiffeners under harmonic pressure loads and in uniform thermal environment. The formulation is developed based on the higher-order shear deformation theory (HSDT) combined with von Kármán-type nonlinear kinematics. An enhanced smeared stiffener approach is employed to incorporate the contribution of stiffeners into the shell's global stiffness. The governing equations are derived using the Lagrangian method, with the Rayleigh dissipation function accounting for energy loss. The harmonic balance method is adopted to determine the stress function, and the nonlinear equations of motion are solved numerically using the Runge–Kutta method. Parametric studies are conducted to assess the effects of CNT distribution, curvature, stiffener orientation, and thermal loading. The results provide key insights into the nonlinear dynamic response of stiffened FG-CNTRC shallow shells, serving as a useful reference for design applications in thermomechanical environments.

**Keywords:** Functionally graded carbon nanotube-reinforced composite, Vibration, Higher-order shear deformation shell theory, Thermal environment, Doubly curved shallow shell.

## 1. Introduction

Recent advances in material science have led to the development of various classes of functionally graded composite materials, such as traditional functionally graded materials (FGMs), carbon nanotube-reinforced composites (FG-CNTRCs), and graphene platelet-reinforced composites (FG-GPLRCs). These novel materials

exhibit superior mechanical, thermal, and multifunctional characteristics due to the continuous variation of their constituents across the thickness. Their high strength-to-weight ratio, tunable properties, and enhanced durability make them highly attractive for use in demanding engineering applications, including aerospace structures, thermal barrier systems, and smart materials.

Subsequently, extensive research has been conducted on the thermomechanical behavior of FGM structures to support their practical implementation. The linear buckling and vibration characteristics of FGM plates were examined using classical plate theory (CPT) [1], first-order shear deformation theory (FSDT) [2], and higher-order shear deformation theory (HSDT) [3]. Studies on nonlinear postbuckling, vibrational response, and flutter control of FGM plates employed the perturbation method [4, 5], along with Hamilton's principle in conjunction with supersonic piston aerodynamic theory [6]. Additionally, the quasi-three-dimensional HSDT model was utilized to explore bending and free vibration behaviors of FGM plates with diverse material gradation profiles [7]. Non-polynomial shear deformation theories were also applied to analyze the free and transient vibration responses of FGM plates interacting with elastic foundations [8]. The dynamic behavior of FGM doubly curved shallow shells under free and forced vibrations was addressed through two-dimensional higher-order deformation theories [9], including those with elliptical geometries [10], and by employing the multiple scales method [11]. Furthermore, the nonlinear buckling response of FGM plates and doubly curved shallow shells stiffened with orthogonal or oblique FGM stiffeners was analyzed using FSDT and HSDT, the Galerkin approach, and an enhanced smeared stiffener technique [12–15].

Beyond the aforementioned FGMs, researchers have also focused on nanocomposite systems such as functionally graded carbon nanotube-reinforced composites (FG-CNTRCs), functionally graded graphene-reinforced composites (FG-GRCs), and functionally graded graphene platelet-reinforced composites (FG-GPLRCs). The incorporation of nanoscale reinforcements into the matrix significantly improves the material's mechanical and physical performance, making it highly suitable for advanced engineering applications. The static bending, buckling, and postbuckling responses of FG-GPLRC rectangular plates were explored in various studies [16–18]. Free vibration analyses were carried out for FG-GPLRC plates with standard rectangular shapes, irregular geometries [19], and skew configurations [20], utilizing diverse theoretical models and computational methods. Both linear and nonlinear forced vibration behaviors of FG-GPLRC structures were addressed under harmonic excitation [21], in active vibration control contexts [22], for doubly curved shallow panels [23], and for more geometrically complex curved shells [24, 25]. In the context of FG-CNTRCs, nonlinear bending, buckling, and postbuckling behaviors were examined using HSDT and perturbation techniques [26, 27]. Vibration characteristics of rotating cylindrical FG-CNTRC panels were assessed based on HSDT in combination with the element-free kernel particle Ritz method [28]. Additionally, the dynamic response of FG-CNTRC rectangular and skew plates was studied using the Ritz method with approaches such as the Lagrange multiplier technique [29] and the Gram–Schmidt orthogonalization process within the FSDT framework [30]. Buckling behavior of cracked nanoplates with variable thickness was studied using the FSDT and phase-field technique [31]. The enhanced smeared stiffener approaches for orthogonal and inclined stiffeners were developed to study the nonlinear buckling behavior of FG-CNTRC stiffened plates using HSDT [32-34].

Furthermore, FG-CNTRC sandwich structures incorporating various core configurations were investigated for their free vibration and acoustic insulation characteristics [35]. The FG-CNTRC cylindrical panels with FG-CNTRC multilayer corrugated core were mentioned [36], considering the thermal stresses.

A comprehensive review of existing literature reveals that, although substantial progress has been made in analyzing the mechanical behavior of FGMs and nanocomposite structures, particularly plates and shells reinforced with CNTs or GPLs, most prior studies have focused on simplified geometries, such as flat plates or cylindrical panels. The nonlinear vibration behavior of doubly curved shallow shells made of FG-CNTRC, especially those stiffened with matching FG-CNTRC stiffeners, has received limited attention.

Therefore, despite considerable advancements in the analysis of FG-CNTRC structures, limited studies have addressed the nonlinear free and forced vibration behavior of doubly curved shallow shells stiffened by FG-CNTRC stiffeners under thermal environments and harmonic loads. To bridge this gap, the present study proposes a semi-analytical framework for investigating the geometrically nonlinear vibration of FG-CNTRC stiffened shallow shells exposed to uniform temperature fields. The higher-order shear deformation theory (HSDT), incorporating von Kármán geometric nonlinearity, is employed to derive the governing equations. The contribution of stiffeners is integrated using an improved smeared stiffener technique. The harmonic balance method is utilized to obtain exact stress function solutions, and the nonlinear equations of motion are derived through the application of the Euler–Lagrange formalism with Rayleigh dissipation considered. Numerical simulations are conducted using the Runge-Kutta method to explore the effects of material gradation, stiffening, and thermal conditions on the nonlinear vibration response. The findings provide insights into the dynamic behavior of advanced composite shell structures and offer a valuable reference for design and optimization in thermomechanical environments.

## 2. FG-CNTRC doubly curved shallow shells reinforced by FG-CNTRC stiffeners

An FG-CNTRC doubly curved shallow shell is considered with principal radii of curvature $R_x, R_y$, and in-plane edges $a,b$, thickness $h$, resting on Pasternak elastic foundation. The shell is stiffened by closely spaced FG-CNTRC stiffeners in x- or y-direction, as shown in Fig. 1. The geometrical properties of stiffeners are defined by the stiffener width $b_{stX}$ and $b_{stY}$, the stiffener heights $h_{stX}$ and $h_{stY}$, and stiffener spacings $d_{stX}$ and $d_{stY}$.

Due to the shallowness assumption, a small rise as compared with the span is investigated. Let the $(x,y)$ plane of the quasi-Cartesian coordinate system places at the mid-plane of the shell. In this paper, two types of shallow shells are investigated, the principal radii $R_x = R_y$ corresponds to the spherical shell, and the principal radii $R_x = -R_y$ corresponds to the hyperbolic paraboloid shell.

In this paper, the material properties of FG-CNTRC are assumed to be dependent to the temperature [26, 27]. The volume fractions of CNT for the shell thickness $(-h/2 \le z \le h/2)$ are disposed of through uniform or linear function, as

$$V_{CNT} = \begin{cases} V^*_{CNT} & (UD) \\ \left(\dfrac{4|z|}{h-h_p}\right)V^*_{CNT} & (X) \\ \left(2-\dfrac{4|z|}{h-h_p}\right)V^*_{CNT} & (O) \\ \left(\dfrac{h-2z}{h}\right)V^*_{CNT} & (V) \\ \left(\dfrac{2z+h}{h}\right)V^*_{CNT} & (\Lambda) \end{cases} \quad (1)$$

and for stiffeners $\left(h/2 \le z \le h/2 + h_{st}\right)$

$$V_{CNT} = \begin{cases} V_{CNT}^{*} & (UD) \\ \left[\left|(2h-4z)/h_{st}+2\right|\right]V_{CNT}^{*} & (X) \\ \left[2-\left|(4z-2h)/h_{st}-2\right|\right]V_{CNT}^{*} & (O) \\ \left[2+(h-2z)/h_{st}\right]V_{CNT}^{*} & (V) \\ \left[(2z-h)/h_{st}\right]V_{CNT}^{*} & (\Lambda) \end{cases} \quad (2)$$

The shells and stiffeners are designed according to five distribution patterns of CNTs: UD/UD, X/X, O/O, V/Λ, and Λ/V.

The extended rule of the mixture is adopted to predict the effective elastic constants.

The formulas of Young's moduli, shear moduli, and Poisson's ratio are determined as

$$\begin{aligned} E_{11}^{CNT} &= \eta_1^{CNT} V_{CNT} E_{11}^{CN} + V_M E_M, \\ \frac{\eta_2^{CNT}}{E_{22}^{CNT}} &= \frac{V_{CNT} E_M + V_M E_{22}^{CN}}{E_{22}^{CN} E_M}, \\ \frac{\eta_3^{CNT}}{G_{12}^{CNT}} &= \frac{V_{CNT} G_M + V_M G_{12}^{CN}}{G_{12}^{CN} G_M}, \nu_{12}^{CNT} = V_{CNT}^{*} \nu_{12}^{CN} + V_M \nu_M, \end{aligned} \quad (3)$$

where $V_{CNT}$ and $V_M$ are the volume fractions of the CNTs and the isotropic matrix, with satisfies the relation of $V_{CNT} + V_M = 1$. The Young's and shear moduli of the CNTs are denoted by $E_{11}^{CN}$, $E_{22}^{CN}$ and $G_{12}^{CN}$, $E_M$ and $G_M$ are the corresponding attributives for the polymer matrix and $\eta_j \left(j = 1 \div 3\right)$ are the efficiency parameters of CNTs defined by nanoscale emulations. In addition, Poisson's ratio of the CNT and the isotropic matrix are denoted by $\nu_{12}^{CN}$ and $\nu_M$.

In the $x$- and $y$-directions, the thermal expansion coefficients for shells and stiffeners are presented by

$$\begin{aligned} \alpha_{11}^{CNT} &= V_{CNT}\alpha_{11}^{CN} + V_M \alpha_M, \\ \alpha_{22}^{CNT} &= \left(1+\nu_{12}^{CN}\right)V_{CNT}\alpha_{22}^{CN} \\ &\quad + \left(1+\nu_M\right)V_m\alpha_M - \nu_{12}^{CNT}\alpha_{11}^{CNT}, \end{aligned} \quad (4)$$

where the coefficients of thermal expansion of the CNTs and the isotropic matrix are denoted $\alpha_{11}^{CN}$, $\alpha_{22}^{CN}$ and $\alpha_M$, respectively.

Hooke's law for FG-CNTRC shallow shell taking into account the temperature is defined as follows:

$$\begin{bmatrix} \sigma_x \\ \sigma_y \\ \sigma_{xy} \end{bmatrix} = \begin{bmatrix} \hat{Q}_{11} & \hat{Q}_{12} & 0 \\ \hat{Q}_{12} & \hat{Q}_{22} & 0 \\ 0 & 0 & \hat{Q}_{66} \end{bmatrix} \begin{bmatrix} \varepsilon_x - \alpha_{11}^{CNT}\Delta T \\ \varepsilon_y - \alpha_{22}^{CNT}\Delta T \\ \gamma_{xy} \end{bmatrix}, \quad (5)$$

$$\sigma_{xz} = \hat{Q}_{44}\gamma_{xz}, \quad \sigma_{yz} = \hat{Q}_{55}\gamma_{yz},$$

where $\Delta T$ is the temperature difference from the initial state of the free thermal stress shells to the final state of deformed shells, and the reduced stiffnesses $Q_{ij}$ can be determined

$$\begin{aligned} \hat{Q}_{11} &= \frac{E_{11}^{CNT}}{1-\nu_{12}^{CNT}\nu_{21}^{CNT}}, \ \hat{Q}_{22} = \frac{E_{22}^{CNT}}{1-\nu_{12}^{CNT}\nu_{21}^{CNT}}, \\ \hat{Q}_{12} &= \frac{\nu_{21}^{CNT}E_{11}^{CNT}}{1-\nu_{12}^{CNT}\nu_{21}^{CNT}}, \ \hat{Q}_{44} = \frac{\hat{Q}_{55}}{1.2} = \hat{Q}_{66} = G_{12}^{CNT}. \end{aligned}$$

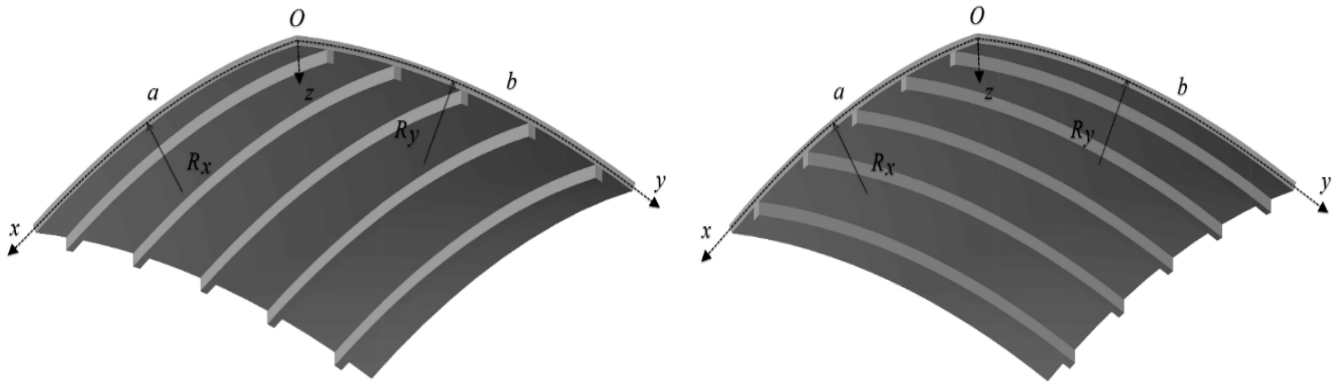


**Fig. 1.** Configurations, quasi-Cartesian coordinate system, and CNT distribution laws of the considered doubly curved shallow shells

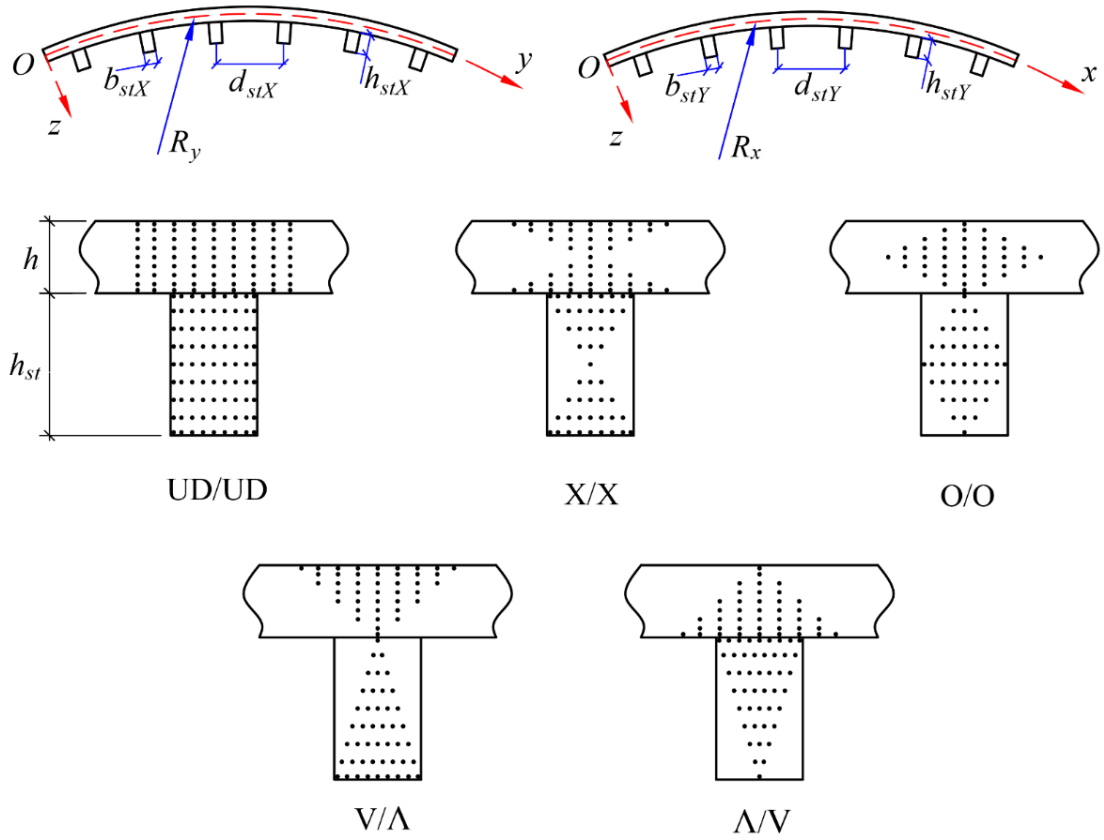


**Fig. 1.** (continued)

## 3. Theoretical formulation

Taking into account the von Karman geometrical nonlinearity, the strain components across the shell thickness at a distance z from the middle surface are presented according to the HSDT, as

$$\begin{Bmatrix}\varepsilon_x\\ \varepsilon_y\\ \gamma_{xy}\end{Bmatrix}=\begin{Bmatrix}\hat{\varepsilon}^*_{0x}\\ \hat{\varepsilon}^*_{0y}\\ \hat{\gamma}^*_{0xy}\end{Bmatrix}+z\begin{Bmatrix}\hat{\varepsilon}^*_{1x}\\ \hat{\varepsilon}^*_{1y}\\ \hat{\gamma}^*_{1xy}\end{Bmatrix}+z^3\begin{Bmatrix}\hat{\varepsilon}^*_{3x}\\ \hat{\varepsilon}^*_{3y}\\ \hat{\gamma}^*_{3xy}\end{Bmatrix},$$

$$\begin{Bmatrix}\gamma_{xz}\\ \gamma_{yz}\end{Bmatrix}=\begin{Bmatrix}\hat{\gamma}^*_{0xz}\\ \hat{\gamma}^*_{0yz}\end{Bmatrix}+z^2\begin{Bmatrix}\hat{\gamma}^*_{2xz}\\ \hat{\gamma}^*_{2yz}\end{Bmatrix}, \quad (6)$$

where

$$\begin{Bmatrix}\hat{\varepsilon}^*_{0x}\\ \hat{\varepsilon}^*_{0y}\\ \hat{\gamma}^*_{0xy}\end{Bmatrix}=\begin{Bmatrix}u_{,x}+w^2_{,x}/2+w_{,x}\bar{w}_{,x}-w/R_x\\ v_{,y}+w^2_{,y}/2+w_{,y}\bar{w}_{,y}-w/R_y\\ v_{,x}+u_{,y}+w_{,x}w_{,y}+w_{,y}\bar{w}_{,x}+w_{,x}\bar{w}_{,y}\end{Bmatrix},$$

$$\begin{Bmatrix}\hat{\varepsilon}^*_{1x}\\ \hat{\varepsilon}^*_{1y}\\ \hat{\gamma}^*_{1xy}\end{Bmatrix}=\begin{Bmatrix}\phi_{x,x}\\ \phi_{y,y}\\ \phi_{y,x}+\phi_{x,y}\end{Bmatrix},\lambda=\frac{4}{3h^2}, \quad (7)$$

$$\begin{Bmatrix}\hat{\varepsilon}^*_{3x}\\ \hat{\varepsilon}^*_{3y}\\ \hat{\gamma}^*_{3xy}\end{Bmatrix}=-\lambda\begin{Bmatrix}w_{,xx}+\phi_{x,x}\\ w_{,yy}+\phi_{y,y}\\ \phi_{y,x}+2w_{,xy}+\phi_{x,y}\end{Bmatrix},$$

$$\begin{Bmatrix}\hat{\gamma}^*_{0xz}\\ \hat{\gamma}^*_{0yz}\end{Bmatrix}=\begin{Bmatrix}w_{,x}+\phi_x\\ w_{,y}+\phi_y\end{Bmatrix},\begin{Bmatrix}\hat{\gamma}^*_{2xz}\\ \hat{\gamma}^*_{2yz}\end{Bmatrix}=-3\lambda\begin{Bmatrix}w_{,x}+\phi_x\\ w_{,y}+\phi_y\end{Bmatrix}.$$

By combining Lekhnitskii's smeared stiffener technique and the higher-order shear deformation anisotropic beam theory, the improved smeared stiffener technique for FG-CNTRC stiffeners is established. The relationships between internal forces and moments with the strains for FG-CNTRC shells stiffened by longitudinal and transversal stiffeners are derived as

$$\begin{aligned}N_x&=\bar{L}_{11}\hat{\varepsilon}^*_{0x}+\bar{L}_{12}\hat{\varepsilon}^*_{0y}+\bar{H}_{11}\hat{\varepsilon}^*_{1x}+\bar{H}_{12}\hat{\varepsilon}^*_{1y}\\&\quad+\bar{G}_{11}\hat{\varepsilon}^*_{3x}+\bar{G}_{12}\hat{\varepsilon}^*_{3y}-\hat{\Phi}_{1x}\Delta T,\\N_y&=\bar{L}_{12}\hat{\varepsilon}^*_{0x}+\bar{L}_{22}\hat{\varepsilon}^*_{0y}+\bar{H}_{12}\hat{\varepsilon}^*_{1x}+\bar{H}_{22}\hat{\varepsilon}^*_{1y}\\&\quad+\bar{G}_{12}\hat{\varepsilon}^*_{3x}+\bar{G}_{22}\hat{\varepsilon}^*_{3y}-\hat{\Phi}_{1y}\Delta T,\\N_{xy}&=\bar{L}_{66}\hat{\gamma}^*_{0xy}+\bar{H}_{66}\hat{\gamma}^*_{1xy}+\bar{G}_{66}\hat{\gamma}^*_{3xy},\end{aligned}$$

$$
\begin{aligned}
M_x &= \bar{H}_{11}\hat{\varepsilon}^*_{0x} + \bar{H}_{12}\hat{\varepsilon}^*_{0y} + \bar{F}_{11}\hat{\varepsilon}^*_{1x} + \bar{F}_{12}\hat{\varepsilon}^*_{1y} \\
&\quad + \bar{A}_{11}\hat{\varepsilon}^*_{3x} + \bar{A}_{12}\hat{\varepsilon}^*_{3y} - \hat{\Phi}_{2x}\Delta T, \\
M_y &= \bar{H}_{12}\hat{\varepsilon}^*_{0x} + \bar{H}_{22}\hat{\varepsilon}^*_{0y} + \bar{F}_{12}\hat{\varepsilon}^*_{1x} + \bar{F}_{22}\hat{\varepsilon}^*_{1y} \\
&\quad + \bar{A}_{12}\hat{\varepsilon}^*_{3x} + \bar{A}_{22}\hat{\varepsilon}^*_{3y} - \hat{\Phi}_{2y}\Delta T, \\
M_{xy} &= \bar{H}_{66}\hat{\gamma}^*_{0xy} + \bar{F}_{66}\hat{\gamma}^*_{1xy} + \bar{A}_{66}\hat{\gamma}^*_{3xy}, \\
T_x &= \bar{G}_{11}\hat{\varepsilon}^*_{0x} + \bar{G}_{12}\hat{\varepsilon}^*_{0y} + \bar{A}_{11}\hat{\varepsilon}^*_{1x} + \bar{A}_{12}\hat{\varepsilon}^*_{1y} \\
&\quad + \bar{D}_{11}\hat{\varepsilon}^*_{3x} + \bar{D}_{12}\hat{\varepsilon}^*_{3y} - \hat{\Phi}_{4x}\Delta T, \\
T_y &= \bar{G}_{12}\hat{\varepsilon}^*_{0x} + \bar{G}_{22}\hat{\varepsilon}^*_{0y} + \bar{A}_{12}\hat{\varepsilon}^*_{1x} + \bar{A}_{22}\hat{\varepsilon}^*_{1y} \\
&\quad + \bar{D}_{12}\hat{\varepsilon}^*_{3x} + \bar{D}_{22}\hat{\varepsilon}^*_{3y} - \hat{\Phi}_{4y}\Delta T, \\
T_{xy} &= \bar{G}_{66}\hat{\gamma}^*_{0xy} + \bar{A}_{66}\hat{\gamma}^*_{1xy} + \bar{D}_{66}\hat{\gamma}^*_{3xy},
\end{aligned} \tag{8}
$$

The shear forces $Q_x, Q_y$ and the higher-order shear forces $S_x, S_y$ are obtained by

$$
\begin{aligned}
Q_x &= \bar{C}_{44}\hat{\gamma}^*_{0xz} + \bar{B}_{44}\hat{\gamma}^*_{2xz}, \\
Q_y &= \bar{C}_{55}\hat{\gamma}^*_{0yz} + \bar{B}_{55}\hat{\gamma}^*_{2yz}, \\
S_x &= \bar{B}_{44}\hat{\gamma}^*_{0xz} + \bar{E}_{44}\hat{\gamma}^*_{2xz}, S_y = \bar{B}_{55}\hat{\gamma}^*_{0yz} + \bar{E}_{55}\hat{\gamma}^*_{2yz}.
\end{aligned} \tag{9}
$$

The stiffnesses and thermal forces in Eqs. (8) and (9) can be displayed as

$$
\begin{aligned}
&\left(\bar{L}_{ij}, \bar{H}_{ij}, \bar{F}_{ij}, \bar{G}_{ij}, \bar{A}_{ij}, \bar{D}_{ij}\right) = \left(\bar{L}^{sh}_{ij}, \bar{H}^{sh}_{ij}, \bar{F}^{sh}_{ij}, \bar{G}^{sh}_{ij}, \bar{A}^{sh}_{ij}, \bar{D}^{sh}_{ij}\right) \\
&+ \left(\bar{L}^{stX}_{ij}, \bar{H}^{stX}_{ij}, \bar{F}^{stX}_{ij}, \bar{G}^{stX}_{ij}, \bar{A}^{stX}_{ij}, \bar{D}^{stX}_{ij}\right) \\
&+ \left(\bar{L}^{stY}_{ij}, \bar{H}^{stY}_{ij}, \bar{F}^{stY}_{ij}, \bar{G}^{stY}_{ij}, \bar{A}^{stY}_{ij}, \bar{D}^{stY}_{ij}\right), \\
&\left(\bar{C}_{ij}, \bar{B}_{ij}, \bar{E}_{ij}\right) = \left(\bar{C}^{sh}_{ij}, \bar{B}^{sh}_{ij}, \bar{E}^{sh}_{ij}\right) + \left(\bar{C}^{stX}_{ij}, \bar{B}^{stX}_{ij}, \bar{E}^{stX}_{ij}\right) \\
&+ \left(\bar{C}^{stY}_{ij}, \bar{B}^{stY}_{ij}, \bar{E}^{stY}_{ij}\right), \\
&\left(\hat{\Phi}_{1x}, \hat{\Phi}_{2x}, \hat{\Phi}_{4x}\right) = \left(\hat{\Phi}^{sh}_{1x}, \hat{\Phi}^{sh}_{2x}, \hat{\Phi}^{sh}_{4x}\right) \\
&+ \left(\hat{\Phi}^{stX}_{1x}, \hat{\Phi}^{stX}_{2x}, \hat{\Phi}^{stX}_{4x}\right) + \left(\hat{\Phi}^{stY}_{1x}, \hat{\Phi}^{stY}_{2x}, \hat{\Phi}^{stY}_{4x}\right), \\
&\left(\hat{\Phi}_{1y}, \hat{\Phi}_{2y}, \hat{\Phi}_{4y}\right) = \left(\hat{\Phi}^{sh}_{1y}, \hat{\Phi}^{sh}_{2y}, \hat{\Phi}^{sh}_{4y}\right) \\
&+ \left(\hat{\Phi}^{stX}_{1y}, \hat{\Phi}^{stX}_{2y}, \hat{\Phi}^{stX}_{4y}\right) + \left(\hat{\Phi}^{stY}_{1y}, \hat{\Phi}^{stY}_{2y}, \hat{\Phi}^{stY}_{4y}\right),
\end{aligned}
$$

with

$$
\begin{aligned}
&\left(\bar{L}^{sh}_{ij}, \bar{H}^{sh}_{ij}, \bar{F}^{sh}_{ij}, \bar{G}^{sh}_{ij}, \bar{A}^{sh}_{ij}, \bar{D}^{sh}_{ij}\right) \\
&= \int_{-h/2}^{h/2} \hat{Q}_{ij}\left(1,\ z, z^2, z^3, z^4, z^6\right) dz, \qquad (i, j = 1,2,6),
\end{aligned}
$$

$$
\left(\bar{C}^{sh}_{ij}, \bar{B}^{sh}_{ij}, \bar{E}^{sh}_{ij}\right) = \int_{-h/2}^{h/2} \hat{Q}_{ij}\left(1, z^2, z^4\right) dz, \qquad (i, j = 4,5),
$$

$$
\left(\bar{C}^{stX}_{ij}, \bar{B}^{stX}_{ij}, \bar{E}^{stX}_{ij}\right) = \frac{b_{stX}}{d_{stX}} \int_{h/2}^{h/2+h_{stX}} \hat{Q}_{ij}\left(1, z^2, z^4\right) dz, (i, j = 4,5),
$$

$$
\left(\bar{C}^{stY}_{ij}, \bar{B}^{stY}_{ij}, \bar{E}^{stY}_{ij}\right) = \frac{b_{stY}}{d_{stY}} \int_{h/2}^{h/2+h_{stY}} \hat{Q}_{ij}\left(1, z^2, z^4\right) dz, (i, j = 4,5),
$$

$$
\left(\hat{\Phi}^{sh}_{1x}, \hat{\Phi}^{sh}_{2x}, \hat{\Phi}^{sh}_{4x}\right) = \int_{-h/2}^{h/2} \left(\hat{Q}_{11}\alpha^{CNT}_{11} + \hat{Q}_{12}\alpha^{CNT}_{22}\right)\left(1, z, z^3\right) dz,
$$

$$
\left(\hat{\Phi}^{stX}_{1x}, \hat{\Phi}^{stX}_{2x}, \hat{\Phi}^{stX}_{4x}\right) =
$$

$$
\frac{b_{stX}}{d_{stX}} \int_{h/2}^{h/2+h_{stX}} \left(\hat{Q}_{11}\alpha^{CNT}_{11} + \hat{Q}_{12}\alpha^{CNT}_{22}\right)\left(1, z, z^3\right) dz,
$$

$$
\left(\hat{\Phi}^{stY}_{1x}, \hat{\Phi}^{stY}_{2x}, \hat{\Phi}^{stY}_{4x}\right) =
$$

$$
\frac{b_{stY}}{d_{stY}} \int_{h/2}^{h/2+h_{stY}} \left(\hat{Q}_{11}\alpha^{CNT}_{11} + \hat{Q}_{12}\alpha^{CNT}_{22}\right)\left(1, z, z^3\right) dz,
$$

$$
\left(\hat{\Phi}^{sh}_{1y}, \hat{\Phi}^{sh}_{2y}, \hat{\Phi}^{sh}_{4y}\right) = \int_{-h/2}^{h/2} \left(\hat{Q}_{12}\alpha^{CNT}_{11} + \hat{Q}_{22}\alpha^{CNT}_{22}\right)\left(1, z, z^3\right) dz,
$$

$$
\left(\hat{\Phi}^{stX}_{1y}, \hat{\Phi}^{stX}_{2y}, \hat{\Phi}^{stX}_{4y}\right) =
$$

$$
\frac{b_{stX}}{d_{stX}} \int_{h/2}^{h/2+h_{stX}} \left(\hat{Q}_{11}\alpha^{CNT}_{11} + \hat{Q}_{12}\alpha^{CNT}_{22}\right)\left(1, z, z^3\right) dz,
$$

$$
\left(\hat{\Phi}^{stY}_{1y}, \hat{\Phi}^{stY}_{2y}, \hat{\Phi}^{stY}_{4y}\right) =
$$

$$
\frac{b_{stY}}{d_{stY}} \int_{h/2}^{h/2+h_{stY}} \left(\hat{Q}_{11}\alpha^{CNT}_{11} + \hat{Q}_{12}\alpha^{CNT}_{22}\right)\left(1, z, z^3\right) dz,
$$

The stiffness components of X stiffeners $\bar{L}^{stX}_{ij}, \bar{H}^{stX}_{ij}, \bar{F}^{stX}_{ij}, \bar{G}^{stX}_{ij}, \bar{A}^{stX}_{ij}, \bar{D}^{stX}_{ij}$ are presented as

$$
\begin{bmatrix}
\bar{L}^{stX}_{11} & \bar{H}^{stX}_{11} & \bar{G}^{stX}_{11} \\
\bar{H}^{stX}_{11} & \bar{F}^{stX}_{11} & \bar{A}^{stX}_{11} \\
\bar{G}^{stX}_{11} & \bar{A}^{stX}_{11} & \bar{D}^{stX}_{11}
\end{bmatrix} =
\begin{bmatrix}
L_{11} & H_{11} & G_{11} \\
H_{11} & F_{11} & A_{11} \\
G_{11} & A_{11} & D_{11}
\end{bmatrix}
$$

$$
-
\begin{bmatrix}
L_{12} & 0 & H_{12} & 0 & G_{12} & 0 \\
H_{12} & 0 & F_{12} & 0 & A_{12} & 0 \\
G_{12} & 0 & A_{12} & 0 & D_{12} & 0
\end{bmatrix}
$$

$$
\times
\begin{bmatrix}
L_{22} & 0 & H_{22} & 0 & G_{22} & 0 \\
0 & L_{66} & 0 & H_{66} & 0 & G_{66} \\
H_{22} & 0 & F_{22} & 0 & A_{22} & 0 \\
0 & H_{66} & 0 & F_{66} & 0 & A_{66} \\
G_{22} & 0 & A_{22} & 0 & G_{66} & 0 \\
0 & D_{22} & 0 & A_{66} & 0 & D_{66}
\end{bmatrix}^{-1}
$$

$$\times\begin{bmatrix} L_{12} & H_{12} & G_{12} \\ 0 & 0 & 0 \\ H_{12} & F_{12} & A_{12} \\ 0 & 0 & 0 \\ G_{12} & A_{12} & D_{12} \\ 0 & 0 & 0 \end{bmatrix},$$

$$\left(L_{ij},H_{ij},F_{ij},G_{ij},A_{ij},D_{ij}\right)= \int_{h/2}^{h/2+h_{stX}} \hat{Q}_{ij}\left(1,\ z,z^2,z^3,z^4,z^6\right)dz,(i,j=1,2,6),$$

Apply the same procedure as above to determine the stiffnesses of Y stiffeners $\bar{L}_{ij}^{stY},\bar{H}_{ij}^{stY},\bar{F}_{ij}^{stY},\bar{G}_{ij}^{stY},\bar{A}_{ij}^{stY},\bar{D}_{ij}^{stY}$.

The compatibility equation deduced from Eq. (7) is in the form of

$$\begin{aligned}&\hat{\varepsilon}_{0x,yy}^{*}+\hat{\varepsilon}_{0y,xx}^{*}-\hat{\gamma}_{0xy,xy}^{*}= \\ &-\bar{w}_{,xx}w_{,yy}+2w_{,xy}\bar{w}_{,xy} \\ &+w_{,xy}^{2}-w_{,xx}w_{,yy} \\ &-w_{,xx}\bar{w}_{,yy}-\frac{w_{,xx}}{R_y}-\frac{w_{,yy}}{R_x}.\end{aligned} \tag{10}$$

The introduced stress function $\varsigma(x,y)$ satisfies three following conditions

$$N_x=\varsigma_{,yy},\qquad N_{xy}=-\varsigma_{,xy},\qquad N_y=\varsigma_{,xx}. \tag{11}$$

Rewriting the strain compatibility Eq. (10) with the aid of Eqs. (7, 11), obtained as

$$\begin{aligned}&\bar{L}_{22}^{*}\varsigma_{,xxxx}+\left(\bar{L}_{66}^{*}+2\bar{L}_{12}^{*}\right)\varsigma_{,xxyy}+\bar{L}_{11}^{*}\varsigma_{,yyyy} \\ &+\left(\bar{H}_{21}^{*}-\lambda\bar{G}_{21}^{*}\right)\phi_{x,xxx} \\ &+\left(\lambda\bar{G}_{66}^{*}-\lambda\bar{G}_{11}^{*}+\bar{H}_{11}^{*}-\bar{H}_{66}^{*}\right)\phi_{x,xyy} \\ &+\left(\lambda\bar{G}_{66}^{*}-\lambda\bar{G}_{22}^{*}+\bar{H}_{22}^{*}-\bar{H}_{66}^{*}\right)\phi_{y,xxy} \\ &+\left(\bar{H}_{12}^{*}-\lambda\bar{G}_{12}^{*}\right)\phi_{y,yyy}-\lambda\bar{G}_{21}^{*}w_{,xxxx} \\ &-\lambda\left(\bar{G}_{11}^{*}+\bar{G}_{22}^{*}-2\bar{G}_{66}^{*}\right)w_{,xxyy}-\lambda\bar{G}_{12}^{*}w_{,yyyy} \\ &+w_{,xx}\bar{w}_{,yy}-w_{,xy}^{2}+w_{,xx}w_{,yy}+\bar{w}_{,xx}w_{,yy} \\ &-2w_{,xy}\bar{w}_{,xy}+\frac{w_{,xx}}{R_y}+\frac{w_{,yy}}{R_x}=0,\end{aligned} \tag{12}$$

where

$$\bar{L}_{11}^{*}=\bar{L}_{22}/\left(\bar{L}_{11}\bar{L}_{22}-\bar{L}_{12}^{2}\right),\ \bar{L}_{12}^{*}=-\bar{L}_{12}/\left(\bar{L}_{11}\bar{L}_{22}-\bar{L}_{12}^{2}\right),$$

$$\bar{L}_{22}^{*}=\bar{L}_{11}/\left(\bar{L}_{11}\bar{L}_{22}-\bar{L}_{12}^{2}\right),$$

$$\bar{L}_{66}^{*}=1/\bar{L}_{66},\ \bar{H}_{11}^{*}=\bar{L}_{11}^{*}\bar{H}_{11}+\bar{L}_{12}^{*}\bar{H}_{12},$$

$$\bar{H}_{12}^{*}=\bar{L}_{11}^{*}\bar{H}_{12}+\bar{L}_{12}^{*}\bar{H}_{22},\ \bar{H}_{21}^{*}=\bar{L}_{22}^{*}\bar{H}_{12}+\bar{L}_{12}^{*}\bar{H}_{11},$$

$$\bar{H}_{22}^{*}=\bar{L}_{22}^{*}\bar{H}_{22}+\bar{L}_{12}^{*}\bar{H}_{12},\ \bar{H}_{66}^{*}=\bar{L}_{66}^{*}\bar{H}_{66},\bar{G}_{66}^{*}=\bar{L}_{66}^{*}\bar{G}_{66},$$

$$\bar{G}_{11}^{*}=\bar{L}_{11}^{*}\bar{G}_{11}+\bar{L}_{12}^{*}\bar{G}_{12},\ \bar{G}_{12}^{*}=\bar{L}_{11}^{*}\bar{G}_{12}+\bar{L}_{12}^{*}\bar{G}_{22},$$

$$\bar{G}_{21}^{*}=\bar{L}_{22}^{*}\bar{G}_{12}+\bar{L}_{12}^{*}\bar{G}_{11},\ \bar{G}_{22}^{*}=\bar{L}_{22}^{*}\bar{G}_{22}+\bar{L}_{12}^{*}\bar{G}_{12}.$$

## 4. Solution form, approximate stress function, and solving the problem

In this paper, the FG-CNTRC doubly curved shallow shells are investigated with two boundary conditions.

Firstly, the four edges of the shells are simply supported and freely movable (4F), as

$$\begin{aligned}&N_x=N_{0x}=0,\ T_x=0,\ M_x=0,\\ &N_{xy}=0,\ w=0,\ \phi_y=0\end{aligned}\Big\},\text{at } x=0,a,$$
$$\begin{aligned}&N_y=N_{0y}=0,\ T_y=0,\ M_y=0,\\ &N_{xy}=0,\ w=0,\ \phi_x=0\end{aligned}\Big\},\text{at } y=0,b. \tag{13}$$

Secondly, two edges $x=0,a$ are simply supported and freely movable, and to be simply supported and immovable for two edges $y=0,b$ (2F2I), as

$$\begin{aligned}&N_x=N_{0x}=0,\ T_x=0,\ M_x=0,\\ &N_{xy}=0,\ w=0,\ \phi_y=0\end{aligned}\Big\},\text{at } x=0,a,$$
$$\begin{aligned}&N_y=N_{0y},\ T_y=0,\ M_y=0,\\ &v=0,\ w=0,\ \phi_x=0\end{aligned}\Big\},\text{at } y=0,b. \tag{14}$$

The solution forms for deflection, rotations, and geometrical imperfection are selected to satisfy the three types of boundary conditions, as follows

$$\begin{aligned}&w=W\sin\bar{\alpha}x\sin\bar{\beta}y,\quad w^{*}=\eta h\sin\bar{\alpha}x\sin\bar{\beta}y,\\ &\phi_x=\Phi_x\cos\bar{\alpha}x\sin\bar{\beta}y,\ \phi_y=\Phi_y\sin\bar{\alpha}x\cos\bar{\beta}y,\end{aligned} \tag{15}$$

where $\bar{\alpha}=m\pi/a$, $\bar{\beta}=n\pi/b$, $\eta$ is the imperfection size of the shells, $m$ and $n$ are numbers of half waves in straight and curved directions, respectively.

By substituting the solution form (15) into Eq. (12), after some mathematical manipulations, the stress function can be obtained as follows

$$\varsigma = \frac{1}{2}N_{0y}x^2 + \frac{1}{2}N_{0x}y^2 + \varsigma_1\cos 2\bar{\alpha}x + \varsigma_2\cos 2\bar{\beta}y + \varsigma_3\sin\bar{\alpha}x\sin\bar{\beta}y. \quad (16)$$

with

$$\varsigma_1 = \bar{J}_{11}\left(W + 2\eta h\right)W,\ \ \varsigma_2 = \bar{J}_{21}\left(W + 2\eta h\right)W,\ \ \varsigma_3 = \bar{J}_{31}\Phi_x + \bar{J}_{32}\Phi_y + \bar{J}_{33}W, \quad (17)$$

where

$$\bar{J}_{11} = \frac{\bar{\beta}_1^2}{32\bar{\alpha}_1^2\bar{L}_{22}^*},\quad \bar{J}_{21} = \frac{\bar{\alpha}_1^2}{32\bar{\beta}_1^2\bar{L}_{11}^*},$$

$$\bar{J}_{31} = -\frac{\bar{\alpha}_1\left\{\begin{bmatrix}\left(\bar{G}_{66}^* - \bar{G}_{11}^*\right)\lambda + \bar{H}_{11}^* - \bar{H}_{66}^*\end{bmatrix}\bar{\beta}_1^2 \\ +\bar{\alpha}_1^2\left(-\lambda\bar{G}_{21}^* + \bar{H}_{21}^*\right)\end{bmatrix}\right\}}{\bar{\alpha}_1^4\bar{L}_{22}^* + \bar{\beta}_1^2\left(2\bar{L}_{12}^* + \bar{L}_{66}^*\right)\bar{\alpha}_1^2 + \bar{\beta}_1^4\bar{L}_{11}^*},$$

$$\bar{J}_{32} = -\frac{\bar{\beta}_1\left\{\begin{bmatrix}\left(\bar{G}_{66}^* - \bar{G}_{22}^*\right)\lambda + \bar{H}_{22}^* - \bar{H}_{66}^*\end{bmatrix}\bar{\alpha}_1^2 \\ +\bar{\beta}_1^2\left(-\lambda\bar{G}_{12}^* + \bar{H}_{12}^*\right)\end{bmatrix}\right\}}{\bar{\alpha}_1^4\bar{L}_{22}^* + \bar{\beta}_1^2\left(2\bar{L}_{12}^* + \bar{L}_{66}^*\right)\bar{\alpha}_1^2 + \bar{\beta}_1^4\bar{L}_{11}^*},$$

$$\bar{J}_{33} = \frac{\begin{bmatrix}\lambda\bar{\alpha}_1^4\bar{G}_{21}^* + \lambda\bar{\beta}_1^2\left(\bar{G}_{11}^* + \bar{G}_{22}^* - 2\bar{G}_{66}^*\right)\bar{\alpha}_1^2 \\ +\lambda\bar{\beta}_1^4\bar{G}_{12}^* + \frac{\bar{\alpha}^2}{R_y} + \frac{\bar{\beta}^2}{R_x}\end{bmatrix}}{\bar{\alpha}_1^4\bar{L}_{22}^* + \bar{\beta}_1^2\left(2\bar{L}_{12}^* + \bar{L}_{66}^*\right)\bar{\alpha}_1^2 + \bar{\beta}_1^4\bar{L}_{11}^*}.$$

In the average sense, the immovable condition is expressed as follows

$$\int_0^b\int_0^a v_{,y}dxdy = \bar{k}_{51}W + \bar{k}_{52}\Phi_x + \bar{k}_{53}\Phi_y + \bar{k}_{54}W\left(2\eta h + W\right) + \bar{k}_{55}N_{0x} + \bar{k}_{56}N_{0y} + \bar{k}_{57}\Delta T = 0, \quad (18)$$

where

$$\bar{\zeta}_m = \left(-1\right)^m - 1,\quad \bar{\zeta}_n = \left(-1\right)^n - 1,$$

$$\bar{k}_{51} = \left[1/R_y - \begin{pmatrix}\bar{J}_{33}\bar{\alpha}_1^2\bar{L}_{22}^* + \bar{J}_{33}\bar{\beta}_1^2\bar{L}_{12}^* \\ -\bar{\alpha}_1^2\lambda\bar{G}_{21}^* - \bar{\beta}_1^2\lambda\bar{G}_{22}^*\end{pmatrix}\bar{\zeta}_m\bar{\zeta}_n\right]\Big/\left(\bar{\alpha}_1\bar{\beta}_1\right),$$

$$\bar{k}_{52} = -\left[\begin{bmatrix}\bar{\alpha}_1^2\bar{J}_{31}\bar{L}_{22}^* + \left(\lambda\bar{G}_{21}^* - \bar{H}_{21}^*\right)\bar{\alpha}_1 \\ +\bar{\beta}_1^2\bar{J}_{31}\bar{L}_{12}^*\end{bmatrix}\bar{\zeta}_m\bar{\zeta}_n\right]\Big/\left(\bar{\alpha}_1\bar{\beta}_1\right),$$

$$\bar{k}_{53} = -\left[\begin{bmatrix}\bar{J}_{32}\bar{\beta}_1^2\bar{L}_{12}^* + \left(\lambda\bar{G}_{22}^* - \bar{H}_{22}^*\right)\bar{\beta}_1 \\ +\bar{J}_{32}\bar{\alpha}_1^2\bar{L}_{22}^*\end{bmatrix}\bar{\zeta}_m\bar{\zeta}_n\right]\Big/\left(\bar{\alpha}_1\bar{\beta}_1\right),$$

$$\bar{k}_{54} = -a\bar{\beta}_1^2 b/8,\ \bar{k}_{55} = ba\bar{L}_{12}^*,\ \bar{k}_{56} = ba\bar{L}_{22}^*,$$

$$\bar{k}_{57} = ab\left(\bar{L}_{12}^*\hat{\Phi}_{1x} + \bar{L}_{22}^*\hat{\Phi}_{1y}\right),$$

The total energy of the shells can be calculated through the kinetic energy, strain energy, and work done by the external loads and foundation interaction, as

$$\hat{\Xi}_{Total} = \hat{\Xi}_t - \hat{\Xi}_{in} + \hat{\Xi}_{ext} = \frac{1}{2}\int_{-h/2}^{h/2}\int_0^b\int_0^a \rho\left(w_{,t} + \bar{w}_{,t}\right)^2 dxdydz + \int_0^b\int_0^a qwdxdy - \frac{1}{2}\int_{-h/2}^{h/2}\int_0^b\int_0^a \begin{bmatrix}\sigma_{xz}\gamma_{xz} + \sigma_{xy}\gamma_{xy} + \sigma_x\left(\varepsilon_x - \alpha_{11}\Delta T\right) \\ +\sigma_y\left(\varepsilon_y - \alpha_{22}\Delta T\right) + \sigma_{yz}\gamma_{yz}\end{bmatrix} \times dxdydz - \int_0^b\int_0^a\left\{\frac{1}{2}w\left[K_1 w - K_2\left(w_{,xx} + w_{,yy}\right)\right]\right\}dxdy. \quad (19)$$

where $K_1$ (N/m$^3$) and $K_2$ (N/m) are the linear stiffnesses of elastic foundations.

The damping potential function using the Rayleigh dissipation function can be presented as

$$d_v = \frac{1}{2}\int_0^b\int_0^a cw_{,t}^2 dxdy. \quad (20)$$

where $c$ is the damping coefficient.

Applying the Euler-Lagrange equations, considering the Rayleigh dissipation function, presented as

$$\frac{d}{dt}\left(\frac{\partial\hat{\Xi}_{Total}}{\partial\dot{W}}\right) - \frac{\partial\hat{\Xi}_{Total}}{\partial W} + \frac{\partial d_v}{\partial\dot{W}} = 0,\quad \frac{d}{dt}\left(\frac{\partial\hat{\Xi}_{Total}}{\partial\dot{\Phi}_x}\right) - \frac{\partial\hat{\Xi}_{Total}}{\partial\Phi_x} = 0,\quad \frac{d}{dt}\left(\frac{\partial\hat{\Xi}_{Total}}{\partial\dot{\Phi}_y}\right) - \frac{\partial\hat{\Xi}_{Total}}{\partial\Phi_y} = 0, \quad (21)$$

leads to

$$\bar{k}_{11}W + \bar{k}_{12}\Phi_x + \bar{k}_{13}\Phi_y + \left(W + \eta h\right) \times\left[\bar{k}_{14}\Phi_x + \bar{k}_{15}\Phi_y + \bar{k}_{17}W\left(W + 2\eta h\right) + \bar{k}_{19}N_{0x}\right] + \bar{k}_{16}W\left(W + 4/3\,\eta h\right) + \bar{k}_{18}N_{0x} + \bar{k}_{110}N_{0y} - \bar{k}_{112}q - \bar{k}_{113}\Delta T + \bar{k}_{115}\ddot{W} + \bar{k}_{116}c\dot{W} = 0, \quad (22)$$

$$\bar{k}_{12}W + \bar{k}_{22}\Phi_x + \bar{k}_{23}\Phi_y + \bar{k}_{24}W\left(W + 2\eta h\right) + \bar{k}_{25}N_{0x} + \bar{k}_{26}N_{0y} - \bar{k}_{27}\Delta T = 0, \quad (23)$$

$$\begin{aligned}&\bar{k}_{13}W+\bar{k}_{23}\Phi_x+\bar{k}_{33}\Phi_y+\bar{k}_{34}W\left(W+2\eta h\right)\\&+\bar{k}_{35}N_{0x}+\bar{k}_{36}N_{0y}-\bar{k}_{37}\Delta T=0,\end{aligned}\tag{24}$$

where

$$\bar{k}_{11}=\frac{ab}{4}\left\{\begin{aligned}&\left(32\bar{L}^*_{22}\bar{J}^2_{12}+\bar{L}^*_{22}\bar{J}^2_{33}+\lambda^2\bar{D}^*_{11}\right)\bar{\alpha}^4_1\\&+\left[\begin{aligned}&\left(\bar{D}^*_{12}+\bar{D}^*_{21}+4\bar{D}^*_{66}\right)\lambda^2\\&+\bar{J}^2_{33}\left(2\bar{L}^*_{12}+\bar{L}^*_{66}\right)\end{aligned}\right]\bar{\alpha}^2_1\bar{\beta}^2_1\\&+\left(9\bar{E}_{44}\lambda^2-6\bar{B}_{44}\lambda+\bar{C}_{44}\right)\bar{\alpha}^2_1\\&+\left(32\bar{L}^*_{11}\bar{J}^2_{22}+\bar{L}^*_{11}\bar{J}^2_{33}+\lambda^2\bar{D}^*_{22}\right)\bar{\beta}^4_1\\&+\left(9\bar{E}_{55}\lambda^2-6\bar{B}_{55}\lambda+\bar{C}_{55}\right)\bar{\beta}^2_1\\&+K_1+K_2\left(\bar{\alpha}^2_1+\bar{\beta}^2_1\right)\\&-32\bar{\zeta}_m\bar{\zeta}_n\bar{J}_{33}\frac{\left[\begin{aligned}&\bar{J}_{12}\bar{L}^*_{22}\bar{\alpha}^4_1+\bar{\beta}^4_1\bar{J}_{22}\bar{L}^*_{11}\\&+\bar{\alpha}^2_1\bar{\beta}^2_1\bar{L}^*_{12}\left(\bar{J}_{12}+\bar{J}_{22}\right)\end{aligned}\right]}{\left(3ab\bar{\alpha}_1\bar{\beta}_1\right)}\end{aligned}\right\},$$

$$\bar{k}_{12}=\frac{ab}{8}\left\{\begin{aligned}&2\bar{J}_{31}\bar{J}_{33}\bar{\alpha}^4_1\bar{L}^*_{22}+\lambda\left(2\lambda\bar{D}^*_{11}-\bar{A}^*_{11}-A^*_{11}\right)\bar{\alpha}^3_1\\&+2\bar{J}_{31}\bar{J}_{33}\bar{\beta}^4_1\bar{L}^*_{11}\\&+\left[\begin{aligned}&\left(\bar{D}^*_{12}+\bar{D}^*_{21}+4\bar{D}^*_{66}\right)\bar{\beta}^2_1\lambda^2\\&+\left(-A^*_{21}-2A^*_{66}-\bar{A}^*_{12}-2\bar{A}^*_{66}\right)\bar{\beta}^2_1\lambda\end{aligned}\right]\bar{\alpha}_1\\&+\left(18\lambda^2\bar{E}_{44}-12\bar{B}_{44}\lambda+2\bar{C}_{44}\right)\bar{\alpha}_1\\&+\bar{\beta}^2_1\left(4\bar{L}^*_{12}+2\bar{L}^*_{66}\right)\bar{J}_{33}\bar{J}_{31}\bar{\alpha}^2_1\\&\frac{-32\left[\begin{aligned}&\bar{J}_{12}\bar{L}^*_{22}\bar{\alpha}^4_1+\bar{J}_{22}\bar{\beta}^4_1\bar{L}^*_{12}\\&+\bar{\alpha}^2_1\bar{\beta}^2_1\left(\bar{J}_{12}+\bar{J}_{22}\right)\bar{L}^*_{12}\end{aligned}\right]\bar{J}_{31}\bar{\zeta}_m\bar{\zeta}_n}{\left(3ab\bar{\alpha}_1\bar{\beta}_1\right)}\end{aligned}\right\},$$

$$\bar{k}_{13}=\frac{ab}{8}\left\{\begin{aligned}&2\bar{J}_{33}\bar{L}^*_{11}\bar{\alpha}_1\bar{\beta}^4_1\bar{J}_{32}+\lambda\left(2\lambda\bar{D}^*_{22}-\bar{A}^*_{22}-A^*_{22}\right)\bar{\beta}^3_1\\&+\bar{\alpha}^2_1\bar{\beta}^2_1\bar{J}_{32}\left(4\bar{L}^*_{12}+2\bar{L}^*_{66}\right)\bar{J}_{33}\\&+2\bar{L}^*_{22}\bar{J}_{33}\bar{J}_{32}\bar{\beta}^4_1\\&+\left[\begin{aligned}&\left(\bar{D}^*_{12}+\bar{D}^*_{21}+4\bar{D}^*_{66}\right)\bar{\alpha}^2_1\lambda^2\\&+\left(-\bar{A}^*_{21}-2\bar{A}^*_{66}-A^*_{12}-2A^*_{66}\right)\bar{\alpha}^2_1\lambda\end{aligned}\right]\bar{\beta}_1\\&+\left(18\lambda^2\bar{E}_{55}-12\lambda\bar{B}_{55}+2\bar{C}_{55}\right)\bar{\beta}_1\\&\frac{-32\left[\begin{aligned}&\bar{J}_{12}\bar{\alpha}^4_1\bar{L}^*_{22}+\bar{J}_{22}\beta^4_1\bar{L}^*_{11}\\&+\bar{L}^*_{12}\bar{\alpha}^2_1\bar{\beta}^2_1\left(\bar{J}_{12}+\bar{J}_{22}\right)\end{aligned}\right]\bar{\zeta}_n\bar{\zeta}_m\bar{J}_{32}}{\left(3ab\bar{\alpha}_1\bar{\beta}_1\right)}\end{aligned}\right\},$$

$$\bar{k}_{14}=-8\left[\begin{aligned}&\bar{J}_{11}\bar{\alpha}^4_1\bar{L}^*_{22}+\bar{\beta}^4_1\bar{J}_{21}\bar{L}^*_{11}\\&+\bar{\alpha}^2_1\bar{\beta}^2_1\left(\bar{J}_{11}+\bar{J}_{21}\right)\bar{L}^*_{12}\end{aligned}\right]\bar{\zeta}_m\bar{\zeta}_n\bar{J}_{31}\Big/\left(3\bar{\alpha}_1\bar{\beta}_1\right),$$

$$\bar{k}_{15}=-8\left[\begin{aligned}&\bar{J}_{11}\bar{\alpha}^4_1\bar{L}^*_{22}+\bar{\beta}^4_1\bar{J}_{21}\bar{L}^*_{11}\\&+\bar{\alpha}^2_1\bar{\beta}^2_1\left(\bar{J}_{11}+\bar{J}_{21}\right)\bar{L}^*_{12}\end{aligned}\right]\bar{\zeta}_m\bar{\zeta}_n\bar{J}_{32}\Big/\left(3\bar{\alpha}_1\bar{\beta}_1\right),$$

$$\bar{k}_{16}=\frac{-4\left[\begin{aligned}&\bar{J}_{11}\bar{\alpha}^4_1\bar{L}^*_{22}+\bar{\beta}^4_1\bar{J}_{21}\bar{L}^*_{11}\\&+\bar{\alpha}^2_1\bar{\beta}^2_1\left(\bar{J}_{11}+\bar{J}_{21}\right)\bar{L}^*_{12}\end{aligned}\right]\bar{\zeta}_m\bar{\zeta}_n\bar{J}_{33}}{\left(\bar{\alpha}_1\bar{\beta}_1\right)}$$
$$+24ab\left(\bar{J}_{11}\bar{J}_{12}\bar{\alpha}^4_1\bar{L}^*_{22}+\bar{J}_{21}\bar{J}_{22}\bar{\beta}^4_1\bar{L}^*_{11}\right),$$

$$\bar{k}_{17}=16ba\left(\bar{J}^2_{11}\bar{\alpha}^4_1\bar{L}^*_{22}+\bar{J}^2_{21}\bar{\beta}^4_1\bar{L}^*_{11}\right),$$

$$\bar{k}_{18}=\lambda\left(\bar{\alpha}^2_1\bar{G}^*_{11}+\bar{\beta}^2_1\bar{G}^*_{12}\right)\bar{\zeta}_m\bar{\zeta}_n\Big/\left(\bar{\alpha}_1\bar{\beta}_1\right),$$

$$\bar{k}_{19}=\bar{\alpha}^2_1ab/4,$$

$$\bar{k}_{110}=-\bar{J}_{33}\left(\bar{\alpha}^2_1\bar{L}^*_{22}+\bar{\beta}^2_1\bar{L}^*_{12}\right)\bar{\zeta}_m\bar{\zeta}_n\Big/\left(\bar{\alpha}_1\bar{\beta}_1\right),$$

$$\bar{k}_{112}=\bar{\zeta}_m\bar{\zeta}_n\Big/\left(\bar{\alpha}_1\bar{\beta}_1\right),$$

$$\bar{k}_{113}=\frac{-\left[\begin{aligned}&\left(\bar{G}^*_{11}\hat{\Phi}_{1x}+\bar{G}^*_{21}\hat{\Phi}_{1y}-\hat{\Phi}_{4x}\right)\bar{\alpha}^2_1\\&+\bar{\beta}^2_1\left(\bar{G}^*_{12}\hat{\Phi}_{1x}+\bar{G}^*_{22}\hat{\Phi}_{1y}-\hat{\Phi}_{4y}\right)\end{aligned}\right]\lambda\bar{\zeta}_m\bar{\zeta}_n}{\left(\bar{\alpha}_1\bar{\beta}_1\right)},$$

$$\bar{k}_{115}=\frac{ab}{4}\left[\begin{aligned}&\int_{-h/2}^{h/2}\left(V_{CNT}\rho_{CNT}+V_M\rho_M\right)dz\\&+\frac{b_{stX}}{d_{stX}}\int_{h/2}^{h/2+h_{stX}}\left(V_{CNT}\rho_{CNT}+V_M\rho_M\right)dz\\&+\frac{b_{stY}}{d_{stY}}\int_{h/2}^{h/2+h_{stY}}\left(V_{CNT}\rho_{CNT}+V_M\rho_M\right)dz\end{aligned}\right],$$

$$\bar{k}_{116}=ab/4,$$

$$\bar{k}_{22}=\frac{ab}{4}\left\{\begin{aligned}&\left[\bar{L}^*_{22}\bar{\alpha}^4_1+\bar{\beta}^4_1\bar{L}^*_{11}+\bar{\alpha}^2_1\bar{\beta}^2_1\left(2\bar{L}^*_{12}+\bar{L}^*_{66}\right)\right]\bar{J}^2_{31}\\&+\left[\lambda^2\bar{D}^*_{11}+\left(-\bar{A}^*_{11}-A^*_{11}\right)\lambda+\bar{F}^*_{11}\right]\bar{\alpha}^2_1\\&+\left[\lambda^2\bar{D}^*_{66}+\left(-\bar{A}^*_{66}-A^*_{66}\right)\lambda+\bar{F}^*_{66}\right]\bar{\beta}^2_1\\&+9\bar{E}_{44}\lambda^2-6\bar{B}_{44}\lambda+\bar{C}_{44}\end{aligned}\right\},$$

$$\bar{k}_{23}=\frac{ab}{4}\left\{\begin{aligned}&\left[\bar{L}^*_{22}\bar{\alpha}^4_1+\left(2\bar{L}^*_{12}+\bar{L}^*_{66}\right)\bar{\alpha}^2_1\bar{\beta}^2_1+\bar{L}^*_{11}\bar{\beta}^4_1\right]\bar{J}_{32}\bar{J}_{31}\\&+\frac{1}{2}\bar{\alpha}_1\bar{\beta}_1\left[\left(\bar{D}^*_{12}+\bar{D}^*_{21}+2\bar{D}^*_{66}\right)\lambda^2+\bar{F}^*_{21}+\bar{F}^*_{12}\right.\\&\left.+2\bar{F}^*_{66}+\left(\begin{aligned}&-\bar{A}^*_{12}-\bar{A}^*_{21}-2\bar{A}^*_{66}\\&-A^*_{12}-A^*_{21}-2A^*_{66}\end{aligned}\right)\lambda\right]\end{aligned}\right\},$$

$$\bar{k}_{24} = -4\begin{pmatrix} \bar{J}_{11}\bar{\alpha}_1^4\bar{L}^*_{22} + \bar{\beta}_1^4\bar{J}_{21}\bar{L}^*_{11} \\ +\bar{\alpha}_1^2\bar{\beta}_1^2\left(\bar{J}_{11}+\bar{J}_{21}\right)\bar{L}^*_{12} \end{pmatrix}\bar{J}_{31}\bar{\zeta}_n\bar{\zeta}_m \Big/ \left(\bar{\alpha}_1\bar{\beta}_1\right),$$

$$\bar{k}_{25} = -\left(\bar{H}^*_{11} - \bar{G}^*_{11}\lambda\right)\bar{\zeta}_n\bar{\zeta}_m \Big/ \bar{\beta}_1,$$

$$\bar{k}_{26} = -\left(\bar{\alpha}_1^2\bar{L}^*_{22} + \bar{\beta}_1^2\bar{L}^*_{12}\right)\bar{J}_{31}\bar{\zeta}_n\bar{\zeta}_m \Big/ \left(\bar{\alpha}_1\bar{\beta}_1\right),$$

$$\bar{k}_{27} = \begin{bmatrix} \left(-\bar{G}^*_{11}\hat{\Phi}_{1x} - \bar{G}^*_{21}\hat{\Phi}_{1y} + \hat{\Phi}_{4x}\right)\lambda \\ +\bar{H}^*_{21}\hat{\Phi}_{1y} + \bar{H}^*_{11}\hat{\Phi}_{1x} - \hat{\Phi}_{2y} \end{bmatrix}\bar{\zeta}_m\bar{\zeta}_n \Big/ \bar{\beta}_1,$$

$$\bar{k}_{33} = \frac{ab}{4}\begin{Bmatrix} \left[\bar{L}^*_{22}\bar{\alpha}_1^4 + \bar{\beta}_1^4\bar{L}^*_{11} + \bar{\alpha}_1^2\bar{\beta}_1^2\left(2\bar{L}^*_{12} + \bar{L}^*_{66}\right)\right]\bar{J}^2_{32} \\ +\left[\lambda^2\bar{D}^*_{22} + \left(-\bar{A}^*_{22} - A^*_{22}\right)\lambda + \bar{F}^*_{22}\right]\bar{\beta}_1^2 \\ +\left[\lambda^2\bar{D}^*_{66} + \left(-\bar{A}^*_{66} - A^*_{66}\right)\lambda + \bar{F}^*_{66}\right]\bar{\alpha}_1^2 \\ +9\bar{E}_{55}\lambda^2 - 6\bar{B}_{55}\lambda + \bar{C}_{55} \end{Bmatrix},$$

$$\bar{k}_{34} = -4\begin{bmatrix} \bar{J}_{11}\bar{\alpha}_1^4\bar{L}^*_{22} + \bar{\beta}_1^4\bar{J}_{21}\bar{L}^*_{11} \\ +\bar{\alpha}_1^2\bar{\beta}_1^2\left(\bar{J}_{11}+\bar{J}_{21}\right)\bar{L}^*_{12} \end{bmatrix}\bar{J}_{32}\bar{\zeta}_n\bar{\zeta}_m \Big/ \left(3\bar{\alpha}_1\bar{\beta}_1\right),$$

$$\bar{k}_{35} = \left(\bar{G}^*_{12}\lambda - \bar{H}^*_{12}\right)\bar{\zeta}_m\bar{\zeta}_n \Big/ \bar{\alpha}_1,$$

$$\bar{k}_{36} = -\bar{J}_{32}\left(\bar{\alpha}_1^2\bar{L}^*_{22} + \bar{\beta}_1^2\bar{L}^*_{12}\right)\bar{\zeta}_m\bar{\zeta}_n \Big/ \left(\bar{\alpha}_1\bar{\beta}_1\right),$$

$$\bar{k}_{37} = \begin{bmatrix} \left(-\bar{G}^*_{12}\hat{\Phi}_{1x} - \bar{G}^*_{22}\hat{\Phi}_{1y} + \hat{\Phi}_{4y}\right)\lambda \\ +\bar{H}^*_{22}\hat{\Phi}_{1y} + \bar{H}^*_{12}\hat{\Phi}_{1x} - \hat{\Phi}_{2y} \end{bmatrix}\bar{\zeta}_m\bar{\zeta}_n \Big/ \bar{\alpha}_1,$$

$$\bar{F}^*_{11} = \bar{F}_{11} - \bar{H}_{11}\bar{H}^*_{11} - \bar{H}_{12}\bar{H}^*_{21},\ \bar{F}^*_{12} = \bar{F}_{12} - \bar{H}_{11}\bar{H}^*_{12} - \bar{H}_{12}\bar{H}^*_{22},$$

$$\bar{F}^*_{66} = \bar{F}_{66} - \bar{H}_{66}\bar{H}^*_{66},\ \bar{F}^*_{21} = \bar{F}_{12} - \bar{H}_{12}\bar{H}^*_{11} - \bar{H}_{22}\bar{H}^*_{21},$$

$$\bar{F}^*_{22} = \bar{F}_{22} - \bar{H}_{12}\bar{H}^*_{12} - \bar{H}_{22}\bar{H}^*_{22},$$

$$\bar{A}^*_{11} = \bar{A}_{11} - \bar{H}_{11}\bar{G}^*_{11} - \bar{H}_{12}\bar{G}^*_{21},$$

$$\bar{A}^*_{12} = \bar{A}_{12} - \bar{H}_{11}\bar{G}^*_{12} - \bar{H}_{12}\bar{G}^*_{22},$$

$$\bar{A}^*_{66} = \bar{A}_{66} - \bar{H}_{66}\bar{G}^*_{66},\ \bar{A}^*_{21} = \bar{A}_{12} - \bar{H}_{12}\bar{G}^*_{11} - \bar{H}_{22}\bar{G}^*_{21},$$

$$\bar{A}^*_{22} = \bar{A}_{22} - \bar{H}_{12}\bar{G}^*_{12} - \bar{H}_{22}\bar{G}^*_{22},$$

$$A^*_{11} = \bar{A}_{11} - \bar{G}_{11}\bar{H}^*_{11} - \bar{G}_{12}\bar{H}^*_{21},$$

$$A^*_{12} = \bar{A}_{12} - \bar{G}_{11}\bar{H}^*_{12} - \bar{G}_{12}\bar{H}^*_{22},$$

$$A^*_{66} = \bar{A}_{66} - \bar{G}_{66}\bar{H}^*_{66},$$

$$A^*_{21} = \bar{A}_{12} - \bar{G}_{12}\bar{H}^*_{11} - \bar{G}_{22}\bar{H}^*_{21},$$

$$A^*_{22} = \bar{A}_{22} - \bar{G}_{12}\bar{H}^*_{12} - \bar{G}_{22}\bar{H}^*_{22},$$

$$\bar{D}^*_{11} = \bar{D}_{11} - \bar{G}_{11}\bar{G}^*_{11} - \bar{G}_{12}\bar{G}^*_{21},$$

$$\bar{D}^*_{12} = \bar{D}_{12} - \bar{G}_{11}\bar{G}^*_{12} - \bar{G}_{12}\bar{G}^*_{22},\ \bar{D}^*_{66} = \bar{D}_{66} - \bar{G}_{66}\bar{G}^*_{66},$$

$$\bar{D}^*_{21} = \bar{D}_{12} - \bar{G}_{12}\bar{G}^*_{11} - \bar{G}_{22}\bar{G}^*_{21},$$

$$\bar{D}^*_{22} = \bar{D}_{22} - \bar{G}_{12}\bar{G}^*_{12} - \bar{G}_{22}\bar{G}^*_{22}.$$

The conditions $N_{0x} = N_{0y} = 0$ are applied for 4F boundary conditions, the motion equation can be established from Eqs. (22-24); Eq. (18) and the condition $N_{0x} = 0$ are applied for 2F2I boundary conditions, the motion equation can be also obtained from Eqs. (22-24), leads to

$$\begin{aligned} &\left(\vartheta_1\bar{o}_{11} + \vartheta_2\bar{o}_{21}\right)W + \left(\vartheta_1\bar{o}_{110} + \vartheta_2\bar{o}_{28}\right)\Delta T \\ &+\bar{k}_{16}W\left(W + 4\eta h/3\right) + \left(2\eta h + W\right) \\ &\times\begin{bmatrix} \left(\vartheta_1\bar{o}_{14} + \vartheta_2\bar{o}_{24}\right)W \\ +\left(\vartheta_1\bar{o}_{15} + \vartheta_2\bar{o}_{25}\right)W\left(W + \eta h\right) \end{bmatrix} \\ &+\left(\eta h + W\right)\begin{bmatrix} \left(\vartheta_1\bar{o}_{12} + \vartheta_2\bar{o}_{22}\right)\Delta T \\ +\left(\vartheta_1\bar{o}_{13} + \vartheta_2\bar{o}_{23}\right)W \end{bmatrix} \\ &-\bar{k}_{112}q + \bar{k}_{115}\ddot{W} + \bar{k}_{116}c\dot{W} = 0, \end{aligned} \tag{25}$$

where, $\vartheta_1 = 1, \vartheta_2 = 0$ for the 4F shells, $\vartheta_1 = 0, \vartheta_2 = 1$ for the 2F2I shells, and

$$\bar{o}_{11} = \bar{k}_{12}\bar{T}_{14} + \bar{k}_{13}\bar{T}_{24} + \bar{k}_{11}, \bar{o}_{12} = \bar{k}_{14}\bar{T}_{15} + \bar{k}_{15}\bar{T}_{25},$$

$$\bar{o}_{13} = \bar{k}_{14}\bar{T}_{14} + \bar{k}_{15}\bar{T}_{24}, \bar{o}_{14} = \bar{k}_{12}\bar{T}_{11} + \bar{k}_{15}\bar{T}_{24},$$

$$\bar{o}_{15} = \bar{k}_{14}\bar{T}_{11} + \bar{k}_{15}\bar{T}_{21} + \bar{k}_{17}, \bar{o}_{16} = \bar{k}_{12}\bar{T}_{13} + \bar{k}_{13}\bar{T}_{23} + \bar{k}_{18},$$

$$\bar{o}_{17} = \bar{k}_{14}\bar{T}_{13} + \bar{k}_{15}\bar{T}_{23} + \bar{k}_{19}, \bar{o}_{18} = \bar{k}_{12}\bar{T}_{12} + \bar{k}_{13}\bar{T}_{22} + \bar{k}_{110},$$

$$\bar{o}_{19} = \bar{k}_{14}\bar{T}_{12} + \bar{k}_{15}\bar{T}_{22}, \bar{o}_{110} = \bar{k}_{12}\bar{T}_{15} + \bar{k}_{13}\bar{T}_{25} - \bar{k}_{113},$$

$$\bar{o}_{21} = \bar{T}_{32}\bar{o}_{18} + \bar{o}_{11},\quad \bar{o}_{22} = \bar{T}_{34}\bar{o}_{19} + \bar{o}_{12},$$

$$\bar{o}_{23} = \bar{T}_{32}\bar{o}_{19} + \bar{o}_{13}, \bar{o}_{24} = \bar{T}_{31}\bar{o}_{18} + \bar{o}_{14},$$

$$\bar{o}_{25} = \bar{T}_{31}\bar{o}_{19} + \bar{o}_{15}, \bar{o}_{26} = \bar{T}_{33}\bar{o}_{18} + \bar{o}_{16},$$

$$\bar{o}_{27} = \bar{T}_{33}\bar{o}_{19} + \bar{o}_{17}, \bar{o}_{28} = \bar{T}_{34}\bar{o}_{18} + \bar{o}_{110},$$

$$\bar{T}_{11} = \frac{\bar{k}_{33}\bar{k}_{24} - \bar{k}_{34}\bar{k}_{23}}{-\bar{k}_{22}\bar{k}_{33} + \bar{k}^2_{23}}, \bar{T}_{12} = -\frac{\bar{k}_{23}\bar{k}_{36} - \bar{k}_{33}\bar{k}_{26}}{-\bar{k}_{22}\bar{k}_{33} + \bar{k}^2_{23}},$$

$$\bar{T}_{13} = -\frac{\bar{k}_{35}\bar{k}_{23} - \bar{k}_{33}\bar{k}_{25}}{-\bar{k}_{22}\bar{k}_{33} + \bar{k}^2_{23}}, \bar{T}_{14} = -\frac{-\bar{k}_{33}\bar{k}_{12} + \bar{k}_{13}\bar{k}_{23}}{-\bar{k}_{22}\bar{k}_{33} + \bar{k}^2_{23}},$$

$$\bar{T}_{15} = \frac{\bar{k}_{37}\bar{k}_{23} - \bar{k}_{33}\bar{k}_{27}}{-\bar{k}_{22}\bar{k}_{33} + \bar{k}^2_{23}}, \bar{T}_{21} = -\frac{-\bar{k}_{34}\bar{k}_{22} + \bar{k}_{23}\bar{k}_{24}}{-\bar{k}_{22}\bar{k}_{33} + \bar{k}^2_{23}},$$

$$\bar{T}_{22} = \frac{\bar{k}_{36}\bar{k}_{22} - \bar{k}_{23}\bar{k}_{26}}{-\bar{k}_{22}\bar{k}_{33} + \bar{k}^2_{23}}, \bar{T}_{23} = \frac{-\bar{k}_{23}\bar{k}_{25} + \bar{k}_{35}\bar{k}_{23}}{-\bar{k}_{22}\bar{k}_{33} + \bar{k}^2_{23}},$$

$$\bar{T}_{24} = \frac{-\bar{k}_{12}\bar{k}_{23} + \bar{k}_{13}\bar{k}_{22}}{-\bar{k}_{22}\bar{k}_{33} + \bar{k}^2_{23}}, \bar{T}_{25} = \frac{-\bar{k}_{22}\bar{k}_{37} + \bar{k}_{23}\bar{k}_{27}}{-\bar{k}_{22}\bar{k}_{33} + \bar{k}^2_{23}},$$

$$\bar{T}_{31} = -\frac{\bar{k}_{52}\bar{T}_{11} + \bar{k}_{53}\bar{T}_{21} + \bar{k}_{54}}{\bar{k}_{52}\bar{T}_{12} + \bar{k}_{53}\bar{T}_{22} + \bar{k}_{56}},$$

$$\bar{T}_{32} = -\frac{\bar{k}_{52}\bar{T}_{14} + \bar{k}_{53}\bar{T}_{24} + \bar{k}_{51}}{\bar{k}_{52}\bar{T}_{12} + \bar{k}_{53}\bar{T}_{22} + \bar{k}_{56}},$$

$$\bar{T}_{33} = -\frac{\bar{k}_{52}\bar{T}_{13} + \bar{k}_{53}\bar{T}_{23} + \bar{k}_{55}}{\bar{k}_{52}\bar{T}_{12} + \bar{k}_{53}\bar{T}_{22} + \bar{k}_{56}},$$

$$\bar{T}_{34} = -\frac{\bar{k}_{52}\bar{T}_{15} + \bar{k}_{53}\bar{T}_{25} + \bar{k}_{57}}{\bar{k}_{52}\bar{T}_{12} + \bar{k}_{53}\bar{T}_{22} + \bar{k}_{56}}.$$

For the forced vibration, the harmonic loads are chosen as a sinusoidal function over time $q = Q\sin\Omega t$ into Eq. (25), and the obtained equation can be solved using the Runge-Kutta method.

The motion equation of free and linear vibration can be obtained by eliminating the nonlinearities. From that, the frequency of free and linear vibration can be obtained as

$$\omega_{mn} = \sqrt{\frac{\left(\vartheta_1\bar{o}_{11} + \vartheta_2\bar{o}_{21} + \left(\vartheta_1\bar{o}_{12} + \vartheta_2\bar{o}_{21}\right)\Delta T\right)}{\bar{k}_{115}}}. \quad (26)$$

Substituting the harmonic solution $W = \varphi\sin(\Omega t)$ to Eq. (25), introducing the dimensionless frequency parameter $\theta = \Omega/\omega_{mn}$, and the like-Galerkin technique is employed, the frequency–amplitude relation is obtained after some simple mathematical transformations, as

$$\theta = \sqrt{1 + \frac{8\varphi\left(\vartheta_1 A_1 + \vartheta_2 B_1\right)}{3\pi} + \frac{3\varphi^2\left(\vartheta_1 A_2 + \vartheta_2 B_2\right)}{4} + \frac{4\Delta T\left(\vartheta_1 A_3 + \vartheta_2 B_3\right)}{\pi\varphi\omega_{mn}^2} + \frac{Q\left(\vartheta_1 A_4 + \vartheta_2 B_4\right)}{\varphi\omega_{mn}^2} - \left(\frac{\bar{k}_{116}c}{\bar{k}_{115}\pi\omega_{mn}}\right)^2} + \frac{\bar{k}_{116}c}{\bar{k}_{115}\pi\omega_{mn}} \quad (27)$$

where

$$A_1 = \frac{\bar{T}_{13} + \bar{T}_{14} + \bar{k}_{16}}{\bar{k}_{115}\omega_{mn}^2},\ A_2 = \frac{\bar{T}_{15}}{\bar{k}_{115}\omega_{mn}^2},$$

$$A_3 = \frac{\bar{T}_{110}}{\bar{k}_{115}},\ A_4 = -\frac{\bar{k}_{112}}{\bar{k}_{115}},$$

$$B_1 = \frac{\bar{T}_{23} + \bar{T}_{24} + \bar{k}_{16}}{\bar{k}_{115}\omega_{mn}^2},\ B_2 = \frac{\bar{T}_{25}}{\bar{k}_{115}\omega_{mn}^2},$$

$$B_3 = \frac{\bar{T}_{28}}{\bar{k}_{115}},\ B_4 = -\frac{\bar{k}_{112}}{\bar{k}_{115}}.$$

## 5. Numerical results and discussions

To validate the present approach, in Table 1, the present results of the fundamental frequency parameters of isotropic doubly curved shallow shells are compared with those of Matsunaga [9], Chorfi and Houmat [10], and Alijani et al. [11]. Perfect agreements are perceived with very small differences between the present and previous results.

Table 2 presents the fundamental frequencies of spherical FG-CNTRC doubly curved shallow shells with and without stiffeners under a uniform temperature rise of 100 K, evaluated for five different CNT distribution patterns and three CNT volume fractions. The results demonstrate a strong influence of material gradation, stiffening configuration, and CNT distribution on the dynamic characteristics of the shells. For unstiffened shells, the fundamental frequency increases with increasing CNT volume fraction, which is consistent across all distribution patterns. Among the patterns, the X/X distribution yields the highest frequencies, indicating its superior stiffness enhancement effect, followed by UD/UD and Λ/V, while O/O consistently exhibits the lowest frequency values. This can be attributed to the spatial variation of stiffness introduced by each CNT gradation scheme. When X-direction stiffeners are applied, a substantial increase in fundamental frequency is observed compared to the unstiffened counterparts, confirming the effectiveness of stiffening in enhancing structural rigidity.

Notably, the V/Λ pattern in the stiffened case achieves the highest frequency values across all CNT volume fractions, showing a synergistic effect between material gradation and stiffener alignment. In contrast, the Λ/V configuration results in the lowest frequency enhancement among the stiffened shells, suggesting a less favorable stiffness distribution between shell and stiffeners. Y-direction stiffeners also contribute to frequency

improvement, though the enhancement is less pronounced than that of the X-direction stiffeners. This directional dependency is likely due to the geometric curvature and boundary constraints in the X and Y directions, where the X stiffeners align more effectively with the dominant curvature-induced stress path. Again, the X/X and V/Λ patterns yield higher frequencies, while the O/O and Λ/V remain the least efficient.

Table 3 presents the fundamental frequencies of doubly curved shallow shells stiffened in the X-direction, subjected to a uniform temperature rise of 100 K, under 2F2I boundary conditions. The results are shown for five CNT distribution patterns and three CNT volume fractions. To ensure accuracy and consistency, three independent sets of numerical calculations are reported, and they exhibit excellent agreement, confirming the robustness of the computational model. As observed in Table 3, the fundamental frequencies increase significantly with increasing CNT volume fraction across all distribution patterns. This behavior is attributed to the improved stiffness of the FG-CNTRC material as the reinforcing phase becomes more dominant. For instance, for the X/X pattern, the frequency increases from approximately 71657.35 rad/s to 105227.18 rad/s as $V^*_{CNT}$ increases from 0.12 to 0.28. Among the five CNT distribution patterns, the V/Λ pattern consistently yields the highest fundamental frequencies across all CNT volume fractions, emphasizing its effectiveness in enhancing dynamic stiffness when both the shell and the stiffeners are graded in complementary directions. In contrast, the Λ/V configuration again produces the lowest frequencies, which may be attributed to a less favorable alignment between material stiffness distribution and structural load path.

Comparing the results in Table 3 with those in Table 2 under 4F boundary conditions, it is evident that the 2F2I boundary condition leads to a modest increase in fundamental frequency, particularly for shells with higher CNT volume fractions. This is likely due to the additional constraints imposed on the shell edges, which limit deformation and thus raise the natural frequency.

Fig. 2 demonstrates the nonlinear frequency–amplitude response of FG-CNTRC doubly curved shallow shells under various conditions, including CNT distribution laws, geometric curvature, stiffener orientation, and excitation amplitude. In Fig. 2a, the effect of CNT distribution patterns (e.g., UD/UD, X/X, O/O, V/Λ, Λ/V) on the nonlinear vibration behavior is investigated. The results indicate that the X/X and V/Λ patterns yield the highest nonlinear frequencies across the amplitude range, suggesting that these distribution laws provide superior stiffness enhancement due to more efficient CNT alignment through the thickness. In contrast, the O/O and Λ/V configurations exhibit significantly lower frequencies, likely due to their less favorable gradation in terms of stiffness contribution.

Fig. 2b analyzes the influence of the principal radii of curvature. Shells with smaller radii (higher curvature) display elevated frequencies and stronger nonlinear characteristics, confirming that increased curvature improves structural rigidity. Conversely, flatter shells (larger radii) experience reduced stiffness, leading to lower vibration frequencies.

Fig. 2c highlights the impact of stiffener orientation. The shells stiffened in the X-direction demonstrate higher frequency responses compared to those stiffened in the Y-direction, emphasizing that stiffener alignment relative to shell curvature is crucial. This directional sensitivity suggests the importance of aligning stiffeners along the primary stress paths to maximize dynamic stiffness. In Fig. 2d, the effect of forced load amplitude is analyzed. As the amplitude of the harmonic excitation increases, the frequency–

amplitude curves exhibit more pronounced nonlinear behavior, with greater deviation from the linear response. This is indicative of hardening-type nonlinear vibration, where the effective stiffness increases with deformation.

Fig. 3 presents the effects of stiffener type and stiffener spacing on the nonlinear dynamic responses of FG-CNTRC doubly curved shallow shells. In Fig. 3a, the influence of stiffener type, specifically, X-direction and Y-direction stiffeners, is evaluated. The results clearly show that X-direction stiffeners lead to significantly lower vibration amplitudes compared to Y-direction stiffeners under the same excitation conditions. This can be attributed to the alignment of the X-stiffeners with the primary load-bearing direction or with the dominant curvature of the shell, allowing them to more effectively constrain transverse displacements and enhance stiffness. In contrast, Y-stiffeners offer less restraint in the deformation path, resulting in larger vibration amplitudes. Fig. 3b examines the role of stiffener spacing. As the spacing between stiffeners decreases, a marked reduction in vibration amplitude is observed. Closer stiffener placement increases the overall stiffness and provides more frequent mechanical constraints along the shell surface, thereby suppressing dynamic deformations more effectively. This demonstrates the beneficial impact of decreasing stiffener spacing in enhancing vibration control.

Fig. 4 illustrates a comprehensive parametric investigation of the nonlinear dynamic responses of stiffened FG-CNTRC doubly curved shallow shells, including the effects of material composition, geometrical dimensions, damping, thermal environment, elastic foundation, and beat phenomenon. In Fig. 4a, the effect of CNT volume fraction on vibration amplitude is examined. As the CNT content increases, the vibration amplitude decreases significantly. This result is attributed to the enhanced stiffness of the FG-CNTRC material with higher reinforcement, which suppresses structural deformation under dynamic loading. Fig. 4b investigates the influence of edge length. An increase in shell dimensions leads to a considerable rise in vibration amplitude. This behavior results from the increased flexibility and mass associated with larger geometrical size, reducing the overall structural stiffness. Fig. 4c shows the role of the damping coefficient. As damping increases, the peak amplitude of vibration responses is gradually reduced, and the system tends to stabilize more rapidly. This is consistent with classical dynamic theory and highlights the importance of damping design in controlling oscillations in practical applications.

In Fig. 4d, the effect of temperature change is evaluated. A slight increase in vibration amplitude is observed as the thermal load increases, which may be attributed to the thermal softening effect of the matrix material in the FG-CNTRC shell. Fig. 4e explores the impact of elastic foundation parameters. Both the Winkler and Pasternak stiffnesses of the foundation significantly influence the vibration amplitude. As the foundation becomes stiffer, the shell experiences reduced amplitude due to the additional reactive forces resisting displacement. Fig. 4f illustrates the beat phenomenon, a nonlinear dynamic feature observed when the excitation frequency approaches the system’s natural frequency. The alternating envelope in the time-history response clearly reveals this phenomenon, which is critical in resonant scenarios.

Fig. 5 illustrates the phase-plane trajectories (deflection–velocity curves) of X-stiffened FG-CNTRC doubly curved shallow shells subjected to harmonic excitation, highlighting the effect of excitation amplitude on the system's dynamic behavior. In Fig. 5a, the shell is subjected to a small-amplitude harmonic load. The phase trajectory forms a single, smooth, closed loop,

indicating a stable periodic motion with a unique attractor. This response is characteristic of a weakly nonlinear or nearly linear regime, where the system exhibits predictable, regular oscillations. The absence of irregularities or bifurcations suggests that the shell vibrates harmonically around its equilibrium configuration. In contrast, Fig. 5b shows the phase diagram when the amplitude of the forced excitation is significantly increased. The trajectory becomes more complex, forming multiple loops and bifurcated paths, which is indicative of strong nonlinear behavior.

**Table 1**. Comparisons of the fundamental frequency parameter $\bar{\omega} = \omega_{mn} h \sqrt{\frac{\rho_c}{E_c}}$ of isotropic doubly curved shallow shells with previous work (4F, $a/b = 1$, $h/a = 0.1$, $m = n = 1$, $\Delta T$ = 0K).

| $a/R_x$ | $b/R_y$ | References | |
|---|---|---|---|
| 0.5 | 0.5 | Alijani et al. [11] | 0.0779 |
| | | Chorfi and Houmat [10] | 0.0762 |
| | | Matsunaga [9] | 0.0751 |
| | | Present | 0.0767 |
| -0.5 | 0.5 | Alijani et al. [11] | 0.0597 |
| | | Chorfi and Houmat [10] | 0.058 |
| | | Matsunaga [9] | 0.0563 |
| | | Present | 0.0581 |

**Table 2**. Fundamental frequencies (rad/s) of spherical shells with and without stiffeners (4F, $h$ =2mm, $a = b = 20h$, $R_x = R_y = a/0.1$, $\eta$ =0, $\Delta T$ =100K, $m = n = 1$, $h_{stX} = h_{stY} = 1.5h$, $b_{stX} = b_{stY} = h$, $d_{stX} = d_{stY} = a/8$, $K_1$ = 10 MN/m$^3$, $K_2$ = 0.1 MN/m)

| | $V^*_{CNT}$ | UD/UD | X/X | O/O | V/Λ | Λ/V |
|---|---|---|---|---|---|---|
| Unstiffened | 0.12 | 36660.29 | 39819.32 | 32116.84 | 34085.43 | 33975.91 |
| | 0.17 | 41915.05 | 46173.30 | 35754.96 | 38402.42 | 38253.03 |
| | 0.28 | 47319.46 | 51853.01 | 39937.58 | 43134.78 | 43039.21 |
| X stiffeners | 0.12 | 70452.28 | 71648.40 | 69033.00 | 79344.37 | 56038.33 |
| | 0.17 | 84767.65 | 86672.07 | 82711.58 | 96837.47 | 66345.79 |
| | 0.28 | 102452.64 | 105216.53 | 100569.47 | 117944.95 | 80647.33 |
| Y stiffeners | 0.12 | 42005.87 | 45975.36 | 36391.31 | 39300.62 | 38026.80 |
| | 0.17 | 50278.26 | 55553.98 | 43110.38 | 47333.70 | 44759.97 |
| | 0.28 | 57477.69 | 63985.64 | 48976.78 | 54442.81 | 51232.61 |

**Table 3**. Fundamental frequencies (rad/s) of X-stiffened doubly curved shallow shells (2F2I, $h$ =2mm, $a = b = 20h$, $R_x = R_y = a/0.1$, $\eta$ =0, $\Delta T$ =100K, $m = n = 1$, $h_{stX} = 1.5h$, $b_{stX} = h$, $d_{stX} = a/8$, $K_1$ = 10 MN/m$^3$, $K_2$ = 0.1 MN/m)

| | $V^*_{CNT}$ | UD/UD | X/X | O/O | V/Λ | Λ/V |
|---|---|---|---|---|---|---|
| $R_x = a/0.1$ | 0.12 | 70460.71 | 71657.35 | 69040.82 | 79353.67 | 56046.97 |
| $R_y = a/0.1$ | 0.17 | 84778.70 | 86683.79 | 82721.82 | 96849.32 | 66358.03 |
| | 0.28 | 102462.72 | 105227.18 | 100578.71 | 117955.51 | 80658.46 |
| $R_x = -a/0.1$ | 0.12 | 70568.96 | 71757.11 | 69160.79 | 79428.42 | 56203.62 |
| $R_y = -a/0.1$ | 0.17 | 84934.87 | 86830.00 | 82896.90 | 96967.37 | 66579.37 |
| | 0.28 | 102602.53 | 105365.81 | 100745.54 | 118075.55 | 80860.42 |
| $R_x = a/0.1$ | 0.12 | 70466.85 | 71658.98 | 69052.27 | 79346.13 | 56066.23 |
| $R_y = -a/0.1$ | 0.17 | 84790.70 | 86690.37 | 82741.69 | 96847.85 | 66384.33 |
| | 0.28 | 102472.19 | 105233.74 | 100598.48 | 117959.86 | 80678.59 |

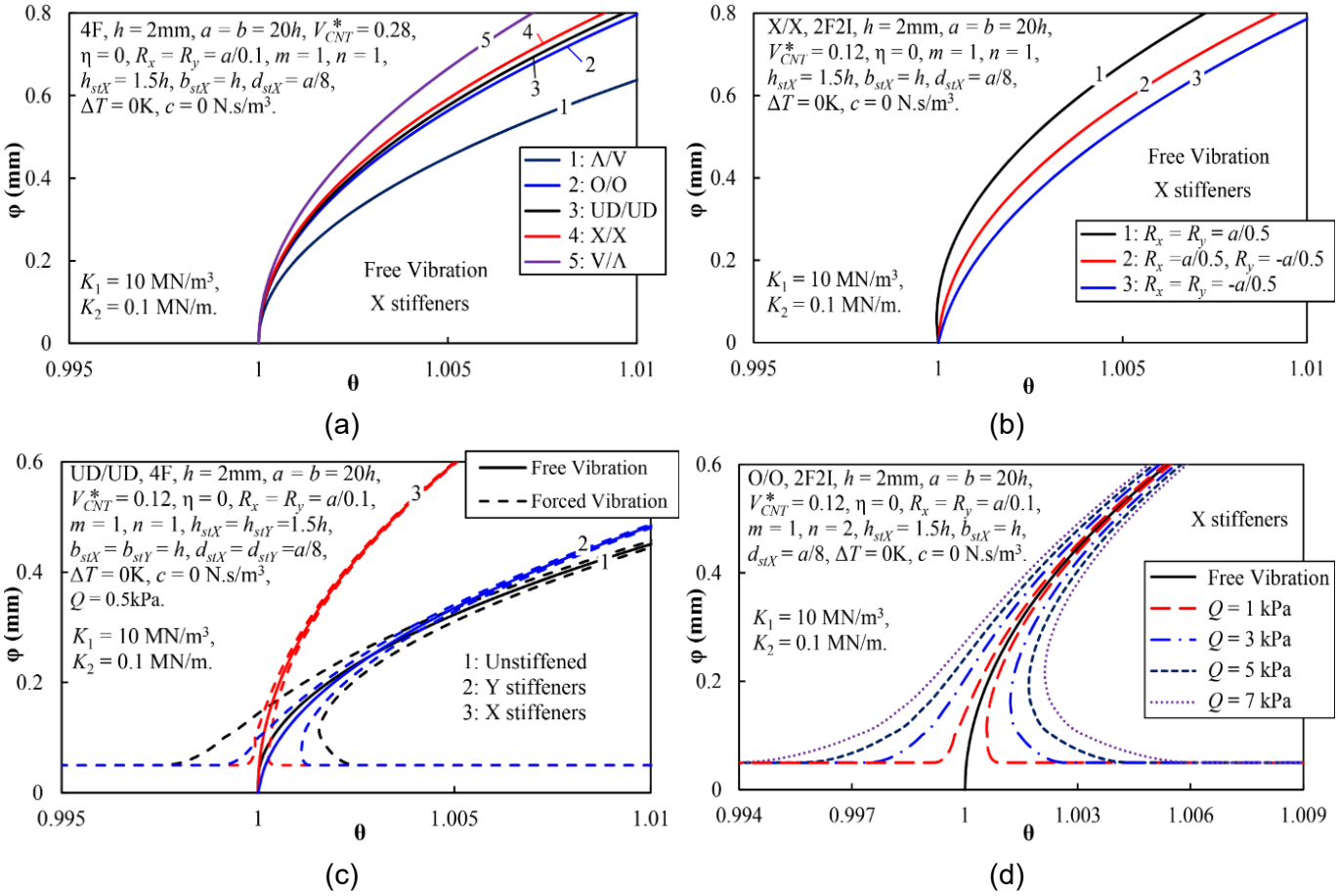


**Fig. 2.** Effects of material, geometrical, stiffener direction, and amplitude of forced load on the frequency-amplitude curves of FG-CNTRC doubly curved shallow shells

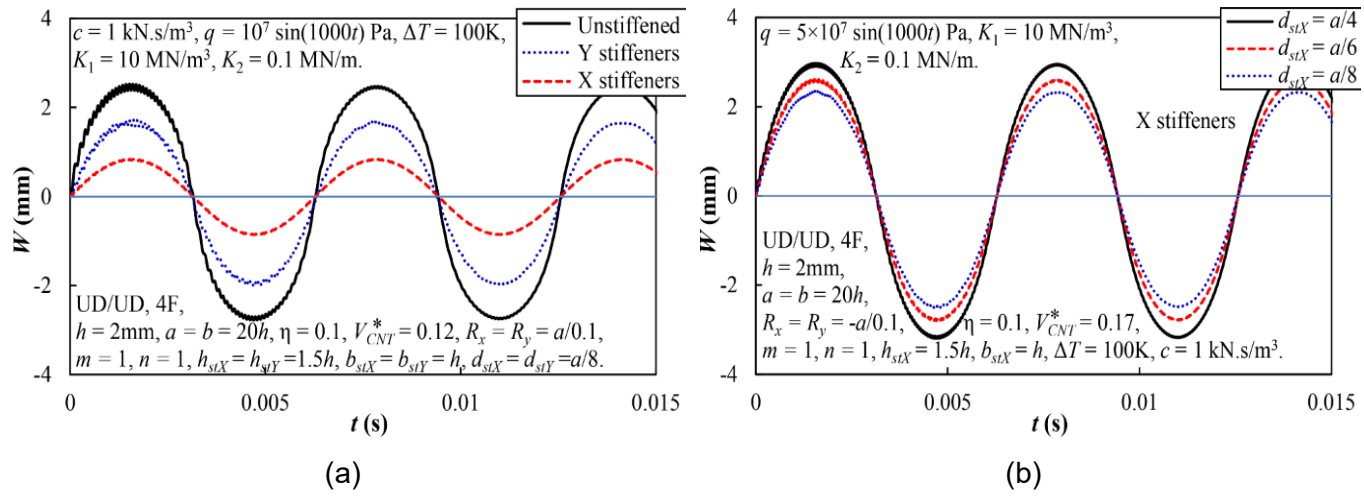


**Fig. 3.** Effects of stiffener type and stiffener spacing on the dynamic responses of FG-CNTRC doubly curved shallow shells

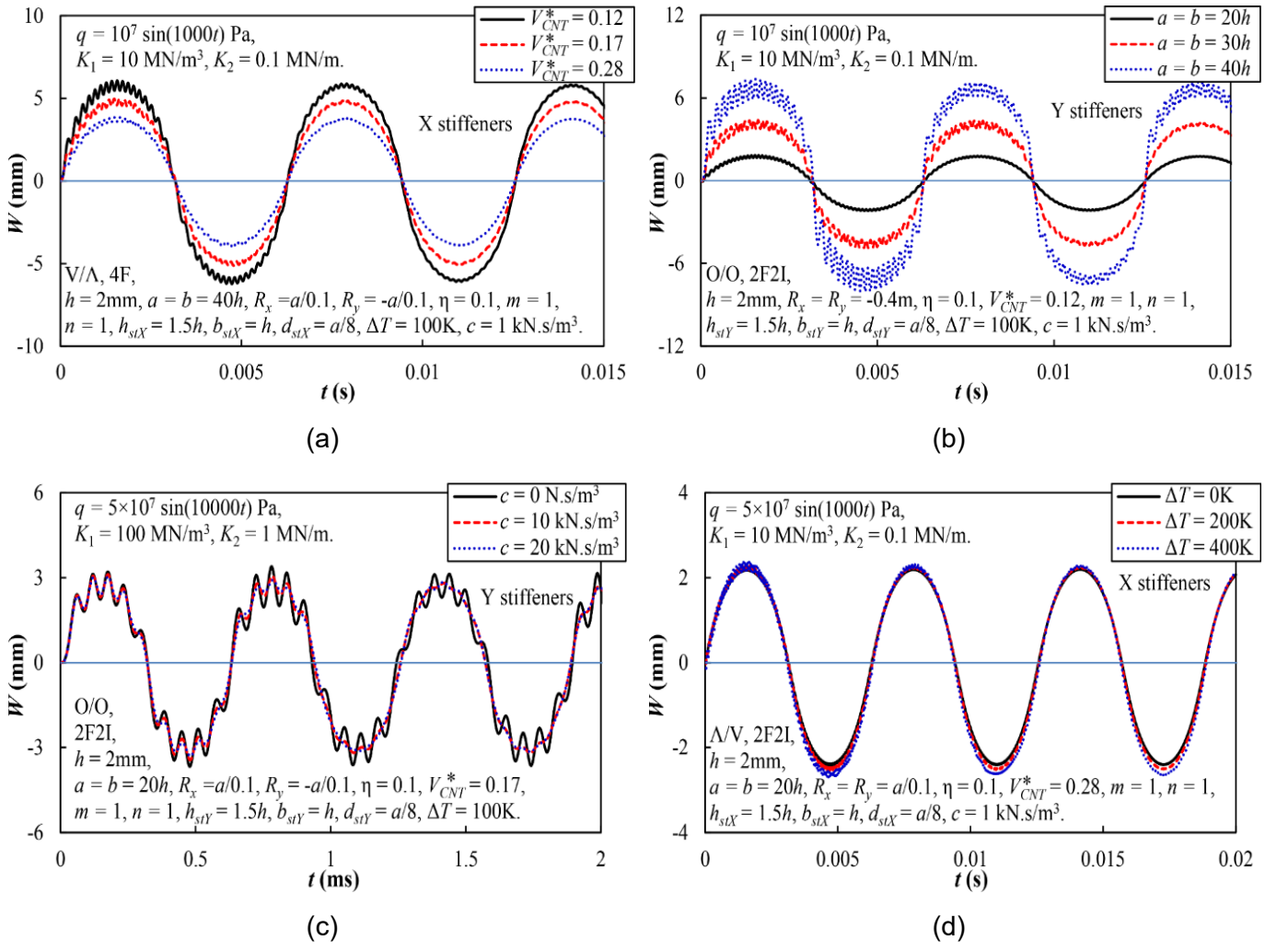


**Fig. 4.** Effects of material, geometrical, temperature change, foundation, and beat phenomenon on the dynamic responses of stiffened FG-CNTRC doubly curved shallow shells

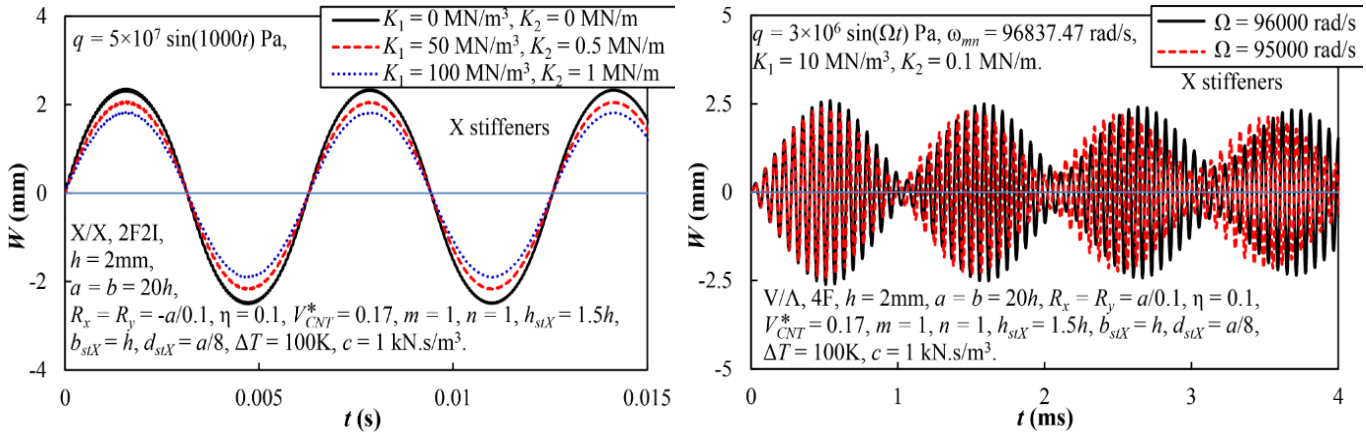


(e) (f)

**Fig. 4.** (continued)

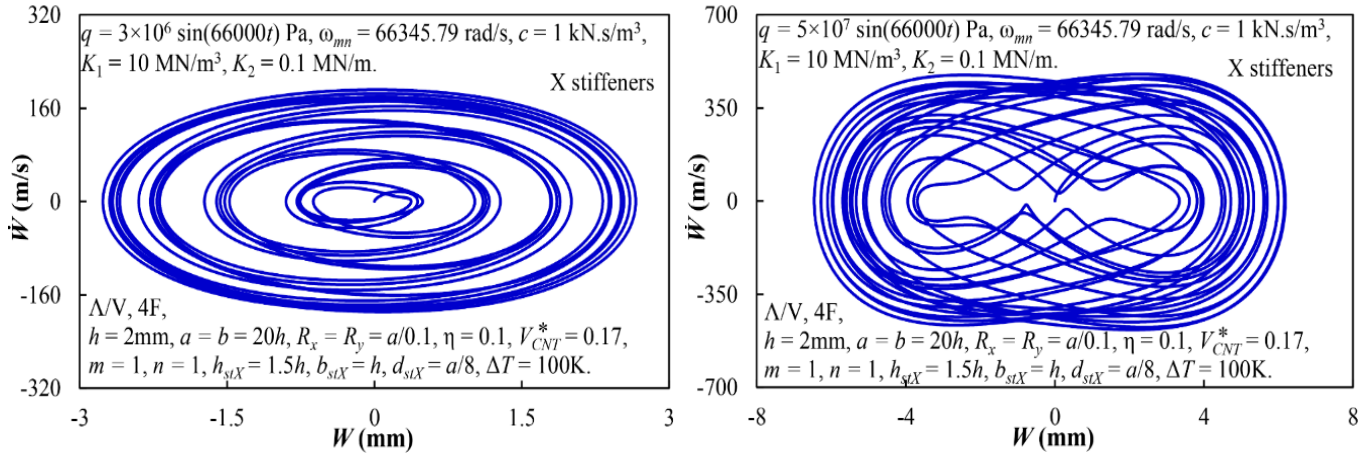


(a) (b)

**Fig. 5.** Phase-plane of X-stiffened FG-CNTRC doubly curved shallow shells

## 6. Conclusions

This study presents a comprehensive semi-analytical framework for analyzing the geometrically nonlinear vibration behavior of FG-CNTRC doubly curved shallow shells stiffened by FG-CNTRC stiffeners in a thermal environment. The governing equations are developed based on the higher-order shear deformation theory (HSDT) and von Kármán nonlinear strain-displacement relations, while an improved smeared stiffener technique is employed to incorporate the stiffening effect of FG-CNTRC stiffeners. The harmonic balance method and energy approach are used to derive the motion equations, and numerical solutions are obtained through the Runge–Kutta method. The main conclusions are summarized as follows:

1) Material gradation and CNT distribution laws significantly influence both the fundamental frequency and the nonlinear vibration response. Among the distribution patterns, the X/X and V/Λ configurations offer superior dynamic stiffness, while the O/O and Λ/V are the least efficient.

2) Stiffeners enhance vibration resistance remarkably, and X-direction stiffeners provide more effective stiffness augmentation compared to Y-direction stiffeners.

3) Geometric parameters, such as curvature

and shell dimensions, strongly affect the nonlinear dynamic behavior. Increased curvature leads to higher stiffness and frequencies, while larger dimensions reduce dynamic rigidity.

4) Thermal effects and foundation parameters must be considered in design, as temperature rise slightly reduces stiffness due to thermal softening, whereas elastic foundation stiffness contributes to suppressing vibration amplitudes.

5) The system exhibits hardening-type nonlinearity under large amplitude excitation. Phase-plane analysis reveals that increased excitation amplitude induces complex nonlinear phenomena such as trajectory bifurcation and multi-stable oscillations.

The findings of this study provide a valuable theoretical foundation for the dynamic analysis and optimal design of advanced composite shell structures. These results can be effectively applied to aerospace, marine, and mechanical systems where lightweight, high-strength materials with tailored vibration characteristics are essential.

**References**

[1] B.A.S. Shariat, R. Javaheri, M.R. Eslami. (2005). Buckling of imperfect functionally graded plates under in-plane compressive loading. *Thin-Walled Structures*, 43(7), 1020-1036.https://doi.org/10.1016/j.tws.2005.01.002

[2] A.M. Zenkour. (2005). A comprehensive analysis of functionally graded sandwich plates: Part 2-Buckling and free vibration. *International Journal of Solids and Structures*, 42(18-19), 5243-5258. https://doi.org/10.1016/j.ijsolstr.2005.02.016

[3] B.A.S. Shariat, M.R. Eslami. (2007). Buckling of thick functionally graded plates under mechanical and thermal loads. *Composite Structures*, 78(3), 433-439. https://doi.org/10.1016/j.compstruct.2005.11.001

[4] H.S. Shen, S.R. Li. (2008). Postbuckling of sandwich plates with FGM face sheets and temperature-dependent properties. *Composites Part B: Engineering*, 39(2), 332-344. https://doi.org/10.1016/j.compositesb.2007.01.004

[5] X.L. Huang, H.S. Shen. (2006). Vibration and dynamic response of functionally graded plates with piezoelectric actuators in thermal environments. *Journal of Sound and Vibration*, 289(1-2), 25-53. https://doi.org/10.1016/j.jsv.2005.01.033

[6] W. Tian, T. Zhao, Y. Gu, Z. Yang. (2022). Nonlinear flutter suppression and performance evaluation of periodically embedded nonlinear vibration absorbers in a supersonic FGM plate. *Aerospace Science and Technology*, 121, 107198.https://doi.org/10.1016/j.ast.2021.107198

[7] K. Bouafia, M.M. Selim, F. Bourada, A.A. Bousahla, M. Bourada, A. Tounsi, E.A.A. Bedia, A. Tounsi. (2021). Bending and free vibration characteristics of various compositions of FG plates on elastic foundation via quasi 3D HSDT model. *Steel and Composite Structures*, 41(4), 487-503. DOI: 10.12989/scs.2021.41.4.487

[8] A.G. Chanda, D.P.N. Kontoni, A.K. Haldar, Z. Guan. (2023). Assessment of non-polynomial shear deformation theories for the free vibration and transient analysis of plates with functionally-graded materials supported on an elastic foundation. *ZAMM - Journal of Applied Mathematics and Mechanics / Zeitschrift für Angewandte Mathematik und Mechanik*, 103(8), e202200487. https://doi.org/10.1002/zamm.202200487

[9] H. Matsunaga. (2008). Free vibration and stability of functionally graded shallow shells according to a 2D higher-order deformation theory. *Composite Structures*, 84(2), 132-146. https://doi.org/10.1016/j.compstruct.2007.07.006

[10] S.M. Chorfi, A. Houmat. (2010). Non-linear

free vibration of a functionally graded doubly-curved shallow shell of elliptical plan-form. *Composite Structures*, 92(10), 2573-2581. https://doi.org/10.1016/j.compstruct.2010.02.001

[11] F. Alijani, M. Amabili, K. Karagiozis, F. Bakhtiari-Nejad. (2011). Nonlinear vibrations of functionally graded doubly curved shallow shells. *Journal of Sound and Vibration*, 330(7), 1432-1454. https://doi.org/10.1016/j.jsv.2010.10.003

[12] D.T. Dong, D.V. Dung. (2019). A third-order shear deformation theory for nonlinear vibration analysis of stiffened functionally graded material sandwich doubly curved shallow shells with four material models. *Journal of Sandwich Structures & Materials*, 21(4), 1316-1356. https://doi.org/10.1177/1099636217715609

[13] V.H. Nam, D.T. Dong, N.T. Phuong, H.D. Tuan. (2019). Nonlinear thermo-mechanical stability of multilayer-FG plates reinforced by orthogonal and oblique stiffeners according to FSDT. *Journal of Reinforced Plastics and Composites*, 38(11), 521-536. https://doi.org/10.1177/0731684419831650

[14] V.H. Nam, N.T. Phuong, D.T. Dong, N.T. Trung, N.V. Tue. (2019). Nonlinear thermo-mechanical buckling of higher-order shear deformable porous functionally graded material plates reinforced by orthogonal and/or oblique stiffeners. *Proceedings of the Institution of Mechanical Engineers, Part C: Journal of Mechanical Engineering Science*, 233(17), 6177-6196. https://doi.org/10.1177/0954406219861658

[15] D.T. Dong, V.H. Nam, N.T. Trung, N.T. Phuong, V.T. Hung. (2022). Nonlinear thermomechanical buckling of sandwich FGM oblique stiffened plates with nonlinear effect of elastic foundation. *Journal of Thermoplastic Composite Materials*, 35(10), 1441-1467. https://doi.org/10.1177/0892705720935957

[16] P. Jiao, Z. Chen, H. Ma, Z. Cheng, Y. Gu, W. Tao. (2024). Post-buckling behavior of rectangular multilayer FG-GPLRC plate with initial geometric defects subjected to non-uniform in-plane compression loads in thermal environment. *Mechanics of Advanced Materials and Structures*, 31(3), 693-712. https://doi.org/10.1080/15376494.2022.2119313

[17] Z.Z. Wang, T. Wang, Y.M. Ding, L.S. Ma. (2024). A simple refined plate theory for the analysis of bending, buckling and free vibration of functionally graded porous plates reinforced by graphene platelets. *Mechanics of Advanced Materials and Structures*, 31(8), 1699-1716. https://doi.org/10.1080/15376494.2022.2141383

[18] P. Jafari, Y. Kiani. (2021). Free vibration of functionally graded graphene platelet reinforced plates: A quasi 3D shear and normal deformable plate model. *Composite Structures*, 275, 114409. DOI: 10.1016/j.compstruct.2021.114409

[19] R. Ansari, R. Hassani, R. Gholami, H. Rouhi. (2021). Free vibration analysis of postbuckled arbitrary-shaped FG-GPL-reinforced porous nanocomposite plates. *Thin-Walled Structures*, 163, 107701. https://doi.org/10.1016/j.tws.2021.107701

[20] Y. Kiani, K.K. Żur. (2022). Free vibrations of graphene platelet reinforced composite skew plates resting on point supports. *Thin-Walled Structures*, 176, 109363. https://doi.org/10.1016/j.tws.2022.109363

[21] R. Gholami, R. Ansari. (2018). Nonlinear harmonically excited vibration of third-order shear deformable functionally graded graphene platelet-reinforced composite rectangular plates. *Engineering Structures*, 156, 197-209. https://doi.org/10.1016/j.engstruct.2017.11.019

[22] B.A. Selim, Z. Liu, K.M. Liew. (2019). Active vibration control of functionally graded graphene nanoplatelets reinforced composite plates integrated with piezoelectric layers. *Thin-*

*Walled Structures*, 145, 106372. DOI: 10.1016/j.tws.2019.106372

[23] A. Wang, H. Chen, Y. Hao, W. Zhang. (2018). Vibration and bending behavior of functionally graded nanocomposite doubly-curved shallow shells reinforced by graphene nanoplatelets. *Results in Physics*, 9, 550-559. https://doi.org/10.1016/j.rinp.2018.02.062

[24] N.T. Phuong, V.M. Duc, N.T. Giang, L.N. Ly, N.T.T. Xuan, V.H. Nam. (2024). Nonlinear Vibration and Dynamic Buckling of Complex Curved Functionally Graded Graphene Panels Reinforced with Inclined Stiffeners. *International Journal of Structural Stability and Dynamics*, 24(19), 2450223. https://doi.org/10.1142/S0219455424502237

[25] V.H. Nam, V.T. Hung, P.N. Nam, V.M. Duc, N.T. Phuong. (2025). Nonlinear electro-thermo-mechanical dynamic behavior of complexly curved GPL-reinforced panels with auxetic core. *Mechanics of Advanced Materials and Structures*, 32(22), 5547-5563. https://doi.org/10.1080/15376494.2024.2425364

[26] H.S. Shen. (2009). Nonlinear bending of functionally graded carbon nanotube-reinforced composite plates in thermal environments. *Composite Structures*, 91(1), 9-19.https://doi.org/10.1016/j.compstruct.2009.04.026

[27] H.S. Shen, Z.H. Zhu. (2010). Buckling and postbuckling behavior of functionally graded nanotube-reinforced composite plates in thermal environments. *Computers, Materials & Continua*, 18(2), 155-182. https://doi.org/10.3970/cmc.2010.018.155

[28] Z.X. Lei, L.W. Zhang, K.M. Liew. (2015). Vibration analysis of CNT-reinforced functionally graded rotating cylindrical panels using the element-free kp-Ritz method. *Composites Part B: Engineering*, 77, 291-303. https://doi.org/10.1016/j.compositesb.2015.03.045

[29] Y. Kiani. (2017). Free vibration of carbon nanotube reinforced composite plate on point Supports using Lagrangian multipliers. *Meccanica*, 52, 1353-1367. https://doi.org/10.1007/s11012-016-0466-3

[30] Y. Kiani. (2016). Free vibration of FG-CNT reinforced composite skew plates. *Aerospace Science and Technology*, 58, 178-188. https://doi.org/10.1016/j.ast.2016.08.018

[31] D.H. Duc, D.V. Thom, P.M. Phuc. (2022). Buckling analysis of variable thickness cracked nanoplates considerting the flexoelectric effect. *Transport and Communications Science Journal*, 73 (5), 470-485. https://doi.org/10.47869/tcsj.73.5.3

[32] T.Q. Minh, V.M. Duc, D.T. Dong, V.H. Nam. (2022). Nonlinear buckling analysis of higher-order shear deformable FG-CNTRC plates stiffened by oblique FG-CNTRC stiffeners. *Vietnam Journal of Mechanics*, 44 (4), 431-444. https://doi.org/10.15625/0866-7136/17933

[33] T.Q. Minh, D.T. Dong, V.T. Hung, C.V. Doan, N.V. Tien, P.T. Hieu. (2024). Geometrically nonlinear buckling of FG-CNTRC plates stiffened by FG-CNTRC stiffeners subjected to combined loads using nonlinear Reddy's HSDT. *International Journal of Structural Stability and Dynamics*, 24(12), 2450133. https://doi.org/10.1142/S0219455424501335

[34] V.M. Duc, T.Q. Minh, N.T. Phuong, V.T. Hung, V.H. Nam. (2024). Nonlinear dynamic responses of CNT-reinforced panels with complex curvature, piezoelectric layer, and CNT-reinforced stiffeners. *European Journal of Mechanics-A/Solids*, 106, 105341. https://doi.org/10.1016/j.euromechsol.2024.105341

[35] Y.Q. Hao, F.L. Li, Y.P. Wang, Y.X. Hao, M. Lv. (2024). Free vibration and sound insulation of FG-CNTRC sandwich plates with different cores. *International Journal of Structural Stability and Dynamics*, 24(11), 2450113. https://doi.org/10.1142/S021945542450113X

[36] V.H. Nam, L.N. Ly, D.T.K. My, N.T. Phuong. (2025). An analytical approach for nonlinear global buckling behavior of sandwich cylindrical panels with multilayer corrugated CNT-reinforced core in thermal environment. *Engineering Structures*, 345(Part B), 121570. https://doi.org/10.1016/j.engstruct.2025.121570